Computers & Fluids xxx (2012) xxx–xxx

Contents lists available at SciVerse ScienceDirect

Computers & Fluids

journal homepage: www.elsevier.com/locate/compfluid

Influence of confinement on obstacle-free turbulent wakes

Luca Biancofiore [a], François Gallaire [b], Richard Pasquetti [a,*]

[a] Laboratoire J.A. Dieudonné, Université de Nice-Sophia Antipolis, Parc Valrose, F-06108 Nice Cedex 02, France
[b] EPFL/LFMI, Route Cantonale, Lausanne, Switzerland

ARTICLE INFO

Article history:
Received 21 June 2011
Received in revised form 15 November 2011
Accepted 12 December 2011
Available online xxxx

Keywords:
Turbulent wakes
Large-eddy simulations
Spectral vanishing viscosity
Confinement

ABSTRACT

Large-eddy simulations (LESs) of obstacle-free wakes, in a channel like geometry with an homogeneous transverse direction, are carried out in order to investigate the influence of confinement on turbulent wakes. The numerical solver makes use of a multi-domain Fourier–Chebyshev spectral method and the LES capability is implemented through a spectral vanishing viscosity technique. A top hat like velocity profile is imposed at the inlet and both no slip and free slip conditions are considered at the confining walls. Prescribing the velocity ratio, defined as the ratio of the velocity gap to the mean velocity, we study the influence of confinement on such flows at the Reynolds number $Re = 5000$. Several quantities are analyzed, as one-dimensional velocity spectra, third order-velocity structure function, turbulent kinetic energy and its dissipation rate. It turns out that for obstacle-free wakes confinement increases the intensity of turbulence and its three-dimensional feature, as e.g. pointed out by Lumley diagrams, in agreement with numerical and experimental results obtained for confined cylinder wake flows. Finally, comparing no slip simulation results with free slip ones, we also point out the role of boundary layers.

1. Introduction

Influence of confinement on wake flows has now a rather long history, starting with Gill [9], who has shown that recessing the central tube of a coaxial injector of rocket engines improves the mixing of the two streams. The mechanisms which take place on coaxial jets are however complex, so that no explanations were given to this phenomenon for more than two decades. Rehab et al. [29] showed, for an unrecessed injector, that a recirculation bubble may appear in the middle of coaxial jets, just like in the wake past an obstacle. Through experiments conducted in a cryogenic test facility [11], it was also shown that the recess enhances the spiral or flapping instability which is characteristic of wakes. Finally, Juniper and Candel [13] related the destabilizing influence of a recess to the enhancement of the instability of the wake in the recessed region of the flow.

From the results of Juniper and Candel [13], numerous studies with aim to understand the influence of confinement on obstacle-free wake flows were undertaken on the basis of both theoretical studies [12,28,4] and numerical simulations [32,5,3]. The former ones have confirmed the destabilizing influence of the confinement, in particular when the blockage is moderate, while the latter have given contrasting results depending on the boundary conditions and the value of Reynolds number. In Biancofiore et al. [5] and Biancofiore [3], the influence of confinement on laminar wakes at medium Reynolds number, i.e. $Re = 100$ and $Re = 500$, was investigated when imposing a top hat velocity profile at the inlet of a two-dimensional channel like geometry. For $Re = 100$, a medium confinement promotes the instability, especially if free slip conditions are considered at the walls. When no slip conditions are implemented, such a destabilizing effect is damped, but persists. For $Re = 500$, more subtle phenomena due to confinement take place, for both boundary conditions. They take the form of a strong instability exhibiting a vacillating wave front. In contrast to the previously cited results, for $100 < Re < 400$ and no slip conditions at the walls no destabilization due to confinement is mentioned in Tammisola et al. [32]. However, only two values of the blockage are compared, which does not allow to investigate extensively the effect of confinement.

Such results help to understand the physics of recessed coaxial injectors, but it is worthwhile to ask what will be the influence of the confinement in a more realistic situation involving a turbulent wake flow. The quality of the mixing is indeed strongly connected to the intensity of the turbulence. It is then of interest to analyze the behaviour of the obstacle-free wake flows investigated in Tammisola et al. [32] and Biancofiore et al. [5] when increasing the Reynolds number, up to e.g. $Re = 5000$. Such high-Reynolds number flows are however out of reach of direct numerical simulations (DNSs), so that large-eddy simulations (LESs) are needed. Since we plan to use a spectral Fourier–Chebyshev numerical method, stabilizing the computations by means of a spectral vanishing viscosity (SVV) technique constitutes a LES approach of interest. Following this SVV–LES approach, we can study how the behaviour of a turbulent wake flow is modified when strengthening the

* Corresponding author.
E-mail address: Richard.PASQUETTI@unice.fr (R. Pasquetti).

0045-7930/$ - see front matter © 2011 Elsevier Ltd. All rights reserved.
doi:10.1016/j.compfluid.2011.12.008

confinement. Note that the present SVV–LES numerical method was already used to compute cylinder/sphere wakes, thermally stratified wakes or for the Ahmed's body flow [26,22].

To the best of our knowledge, there are no experimental or numerical studies concerned with obstacle-free turbulent wake flows submitted to confinement, in contrast to several studies on turbulent confined cylinder wakes. For $10^4 < Re < 10^7$, experiments on confined circular cylinder wakes described in Richter and Naudascher [30] have shown that the confinement is destabilizing. Using LES, similar results were obtained in Kim et al. [15] for confined square cylinder wakes. In particular, these studies show that both the turbulence intensity and the Strouhal number are enhanced as the confinement is increased. Earlier, in Bearman and Zdravkovich [1] experiments were conducted for semi-confined cylinder wakes at $Re = 45{,}000$. It turned out that adding a plate close to the bluff body may regularize the vortex street for certain values of confinement.

Following both previous theoretical analyzes and numerical simulations, the present paper is devoted to confined turbulent obstacle-free wakes. We focus on the flow generated by a top hat velocity profile, with no slip or free slip conditions at the confining walls, as previously analyzed in the laminar case both theoretically [13,12] and numerically [32,3]. With respect to the two-dimensional studies, an homogeneous direction completes the initial setting. Despite its planar geometry, such a model is close to the situation of a real confined wake exiting from a coaxial injector. The outline of the paper is as follows: Section 2 briefly describes the model and the numerical method; Section 3 goes into the details of the influence of the confinement on the turbulent properties of the wake flow; In Section 4, the influence of a free slip boundary condition at the channel walls is considered, while Section 5 focuses on the analysis of the 3D versus 2D nature of the turbulent wake, depending on the confinement parameter. Finally, conclusions are drawn in Section 6.

2. Model and numerical method

The flow is assumed to be governed by the incompressible Navier–Stokes equations. The geometry is channel like and the transverse direction is homogeneous. In the elongated streamwise direction, the approximation in space makes use of a domain decomposition technique. In each subdomain, the spatial approximation is based on a Galerkin Fourier – collocation Chebyshev numerical method. The pressure is only defined at the inner grid-points, so that (i) no boundary conditions are required for the pressure and (ii) the discrete problem is well posed (no "pressure spurious modes"). The time scheme is based on an "Operator Integration Factor" semi-Lagrangian method and a projection technique. Three steps are involved: (i) transport, (ii) diffusion and (iii) projection. Diffusion (resp. transport) terms are handled implicitly (resp. explicitly). In each subdomain, an efficient direct matrix equation solver is used and the interface values are computed using a Schur complement technique. The LES capability is implemented through the use of a SVV technique, which consists of introducing artificial viscosity in the high frequency range of the spectral approximation. The code is vectorized and (weakly) parallelized (one subdomain/processor). Additional details may be found in several papers, see e.g. Cousin and Pasquetti [8], Pasquetti [24], and Minguez et al. [22] and references herein.

In Section 2.1, we first describe the numerical set up. For the sake of completeness, we briefly describe the SVV–LES implementation, in Section 2.2, and provide details on the computation of the dissipation rate of the turbulent kinetic energy in Appendix.

2.1. Numerical set-up

The geometry is channel like in x-streamwise and y-crossflow directions, while the z-spanwise direction is homogeneous. At the sidewalls, no slip (NS) or free slip (FS) conditions are considered. Correspondingly, later on in the text we speak of NS-flows or FS-flows. At the inlet of the channel, one imposes a top hat velocity profile, i.e. $\mathbf{u} = (U, 0, 0)$, with $U(y)$ as shown in Fig. 1. The inner flow has velocity U_1 and width of $2h_1$, while the outer ones have U_2 and h_2. Using as reference scales the average velocity $U_m = (U_1 + U_2)/2$ and the half-width of the inner wake h_1, we introduce non-dimensional quantities, as depicted in Fig. 1. The dimensionless parameters are then: the confinement ratio $h = h_2/h_1$, the velocity ratio $\Lambda = (U_1 - U_2)/(U_1 + U_2)$, and the Reynolds number $Re = (U_1 + U_2)h_1/2\nu$, where ν is the kinematic viscosity. Note that the inlet profile of Fig. 1 was already used in Biancofiore et al. [5] and Biancofiore [3], for DNS of confined laminar wake flows.

In the present work, the velocity ratio $\Lambda = -0.739$ and the Reynolds number $Re = 5000$ are prescribed and we analyze the

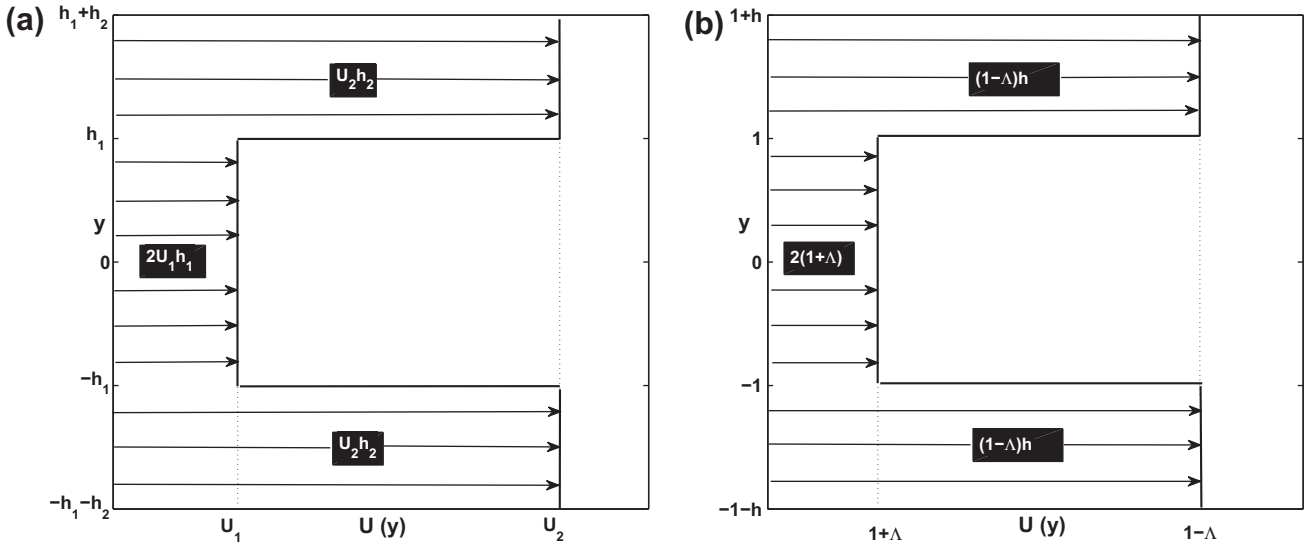

Fig. 1. Schemas of the inlet velocity profile, using dimensioned values (a) and dimensionless values (b). The black squares indicate the flowrates (per unit thickness) that correspond to each part of the flow.

Please cite this article in press as: Biancofiore L et al. Influence of confinement on obstacle-free turbulent wakes. Comput Fluids (2012), doi:10.1016/j.compfluid.2011.12.008

Table 1
Channel flow Reynolds number ($\overline{Re}$), friction Reynolds number (Re_τ), dimensionless distance to the wall (δy) and distance in wall units (δy^+) for the three confinements h.

h	$\overline{Re}$	Re_τ	δy	δy^+
3	54780	1331	0.003552	1.18
1	20000	548	0.002192	0.60
0.7	14783	420	0.001863	0.46

influence of the confinement parameter h for the three different values: $h = 3$,$h = 1$ and $h = 0.7$. The computational domain is $\Omega = (0, L) \times (-H/2, H/2) \times (-E/2, E/2)$, where L, H and E are the length, the height and the thickness of the domain, respectively. The length of the domain is $L = 75$, the thickness E is settled to four times the inner wake, i.e. $E = 8$, and the height H varies with respect to the confinement, i.e. $H = 2(1 + h)$. Such values were already used in Biancofiore et al. [5] in order to detect 3D structures in the flow. We have generally used eight subdomains, and in each of them the polynomial approximation degree in the x- and z-directions are settled to $N_x = 100$ and $N_z = 32$ (64 grid points), respectively. Depending on the height of the domain, we have used $N_y \approx 100$ for the polynomial approximation degree in the y-direction.

One important point is that the inflow profile U of Fig. 1 displays a discontinuity at $y = \pm 1$. Since we are using a spectral method, in order to avoid or at least weaken the Gibbs phenomenon, we use a filtered entry profile. The inlet profile is thus regularized according to:

$$\widetilde{U}_i = \frac{1}{4}(U_{i-1} + 2U_i + U_{i+1}), \tag{1}$$

where U_i (and $\widetilde{U}_i$) are the values at the grid-points of the y-axis. In the frame of a Fourier spectral approximation, it can be shown that this smoothing in physical space is equivalent to a raised cosine filtering. Note that once applied to the top hat profile, the filter changes only the values at the grid-points next to $y = \pm 1$ and, if NS-conditions are imposed, at the first inner grid-point close to the confining walls. Another important point in the present computations is the requirement of soft outflow boundary conditions (OBCs). To this end, we use a convective condition based on the flowrate velocity $\overline{U}$ and a Lagrangian formulation. With n for the time advancement index, at the outlet $x = x_{out}$ we thus enforce:

$$\mathbf{u}(x_{out}, t_{n+1}) = \mathbf{u}(x_{out} - \overline{U}(t_{n+1} - t_n), t_n). \tag{2}$$

Using a Lagrangian rather than an Eulerian formulation allows to localize at best the influence of the OBC. Moreover, (i) with the same goal we use in space a linear interpolation rather than the Chebyshev x-interpolant and (ii) the streamwise outlet profile is slightly adjusted to be consistent with the divergence free constraint, i.e. so that the outlet flowrate exactly equals the inlet one.

The initial condition $\mathbf{u}_0(x, y, z)$ of the three-dimensional LES is given by the final saturated state $\mathbf{u}_f(x, y)$ of the corresponding 2D simulations, i.e. same confinement and velocity ratio, obtained for $Re = 100$ [3]. A random perturbation $\mathbf{u}'(x, y, z)$, of small amplitude, typically 10^{-3}, is added to accelerate the development of a 3D flow, so that

$$\mathbf{u}_0(x, y, z) = \mathbf{u}_f(x, y) + \mathbf{u}'(x, y, z). \tag{3}$$

2.2. SVV–LES formulation

LES methodologies are generally based on the introduction of a stabilizing viscous term resulting from a modeling of the sub-grid stress (SGS) tensor, see e.g. Sagaut [31]. The celebrated Smagorinsky model makes use of a non-linear dissipation term proportional to the Euclidean norm of the strain rate tensor. The SVV technique also uses a dissipation term, but that introduces dissipation only in the high frequency range of the spectral approximation. Especially, this allows to preserve all smooth flows. The SVV technique differs from the spectral viscosity approach [7], for which all scales are affected and is, e.g. more in the spirit of Variational Multi-Scale methods [10]. Note however that both the spectral viscosity (at least in its native form) and the SVV stabilization techniques are linear, whereas LES sub-grid scale models are generally non-linear.

The definition of the SVV stabilizing term V_N is given according to Maday et al. [21], who have resolved in the interval $(-1, 1)$ the inviscid 1D Burgers equation by means of the spectral Legendre method. In this case, with N for the degree of the polynomial approximation, we have

$$V_N = \epsilon_N \partial_x Q_N(\partial_x u_N), \tag{4}$$

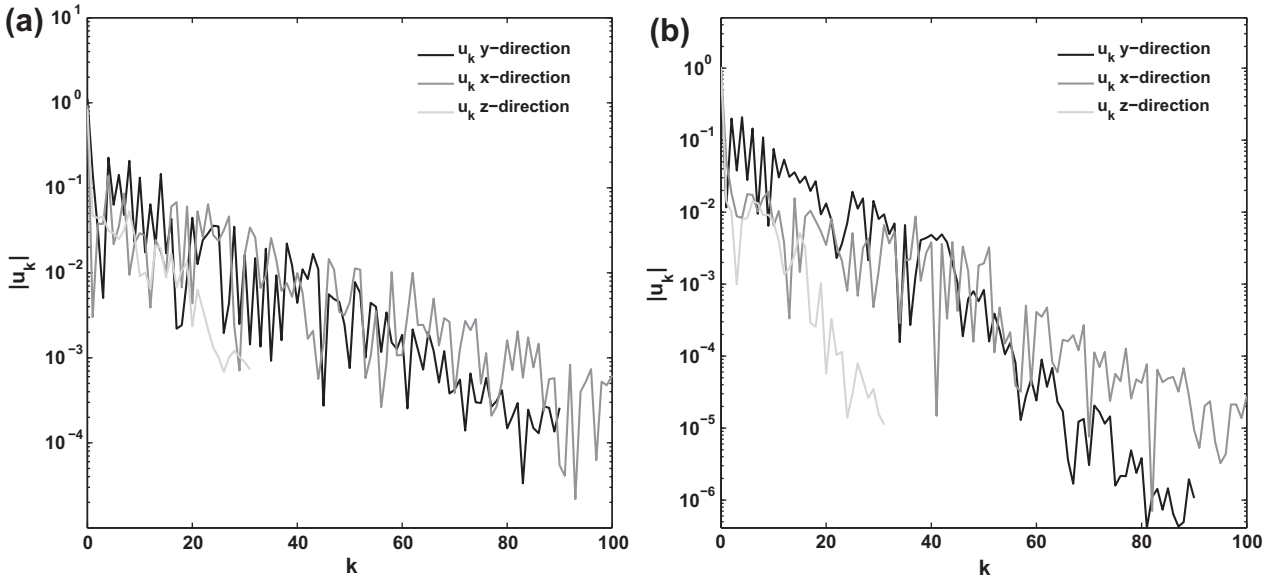

Fig. 2. Chebyshev spectra and modulus of the Fourier spectrum of the streamwise velocity as computed, for $h = 1$, from the x, y and z-axis issued from the points (23.58, 0, 0) (a) and (51.58, 0, 0) (b).

Please cite this article in press as: Biancofiore L et al. Influence of confinement on obstacle-free turbulent wakes. Comput Fluids (2012), doi:10.1016/j.compfluid.2011.12.008

Table 2
Two point-correlations in z-direction, for several distances $l \in (0, E/2)$, of the transverse components of the velocity, as computed for $h = 1$ at the points (23.58, 0, 0) and (51.58, 0, 0).

u-comp.\ l	0.375	1.000	1.625	2.375	3.000	3.625
$v(x = 23.58)$	0.4242	0.0539	0.0258	0.0203	0.0772	0.1010
$w(x = 23.58)$	0.3992	0.0321	0.0091	0.0059	0.0277	0.0276
$v(x = 51.58)$	0.3806	0.2972	0.2935	0.1631	0.1419	0.1404
$w(x = 51.58)$	0.5730	0.1820	0.0009	0.0764	0.0578	0.0094

where u_N is the numerical approximation of some exact solution u, with ϵ_N a $O(N^{-1})$ coefficient and Q_N for the "SVV operator". With L_k for the Legendre polynomial of degree k, it is defined from:

$$Q_N\phi = \sum_{k=0}^{N} \widehat{Q}_k \hat{\phi}_k L_k, \quad \forall \phi \quad \text{such that} \quad \phi = \sum_{k=0}^{N} \hat{\phi}_k L_k, \tag{5}$$

$\widehat{Q}_k = 0$, if $k \leqslant m_N$ and $0 < \widehat{Q}_k \leqslant 1$ if $k > m_N$. As suggested in Maday et al. [21], we use a smooth variation for the coefficients $\widehat{Q}_k$:

$$\widehat{Q}_k = \exp\left(-\left(\frac{N-k}{m_N-k}\right)^2\right), \quad k > m_N. \tag{6}$$

Such a definition of the SVV operator extends naturally to the case of hierarchical basis, and so may be used as it stands for the Fourier (SVV was first defined in this case) or Chebyshev approximations. An extension of the initial definition of the SVV operator, provided for the 1D Burgers equation, to the present 3D Navier–Stokes can be discussed, specially for complex geometries, see Xu and Pasquetti [33]. As proposed in Pasquetti [24], in our multidimensional framework the SVV vector term is written:

$$\mathbf{V}_N = \nabla \cdot \epsilon_N Q_N(\nabla \mathbf{u}_N), \tag{7}$$

where $\epsilon_N Q_N$ is now a diagonal matrix operator, so that the SVV stabilization applies independently in each direction. More precisely, with u_i, V_i for the components of $\mathbf{u}_N$, $\mathbf{V}_N$ and $\epsilon_N Q_N = \mathrm{diag}\{\epsilon_j Q_j\}$, where Q_j is the 1D operator acting in j-direction, we have

$$V_i = \sum_j \partial_j(\epsilon_j Q_j \partial_j u_i). \tag{8}$$

In practice, it is of interest to combine the viscous and SVV stabilizing terms to obtain:

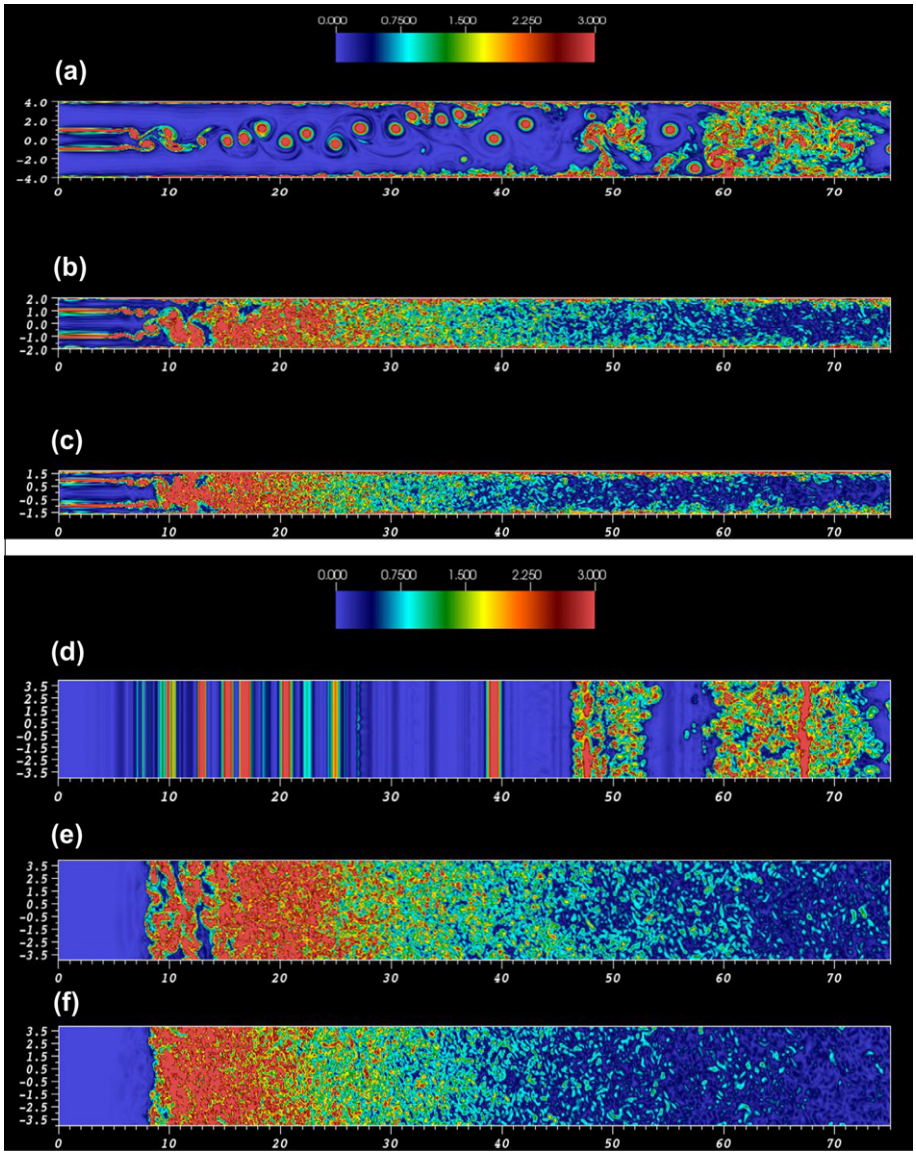

Fig. 3. Instantaneous modulus of the vorticity $|\omega|$ in the central planes $z = 0$ (top) and $y = 0$ (bottom) at $t = 400$ for (a, d) $h = 3$, (b, e) $h = 1$ and (c, f) $h = 0.7$; $Re = 5000$.

Please cite this article in press as: Biancofiore L et al. Influence of confinement on obstacle-free turbulent wakes. Comput Fluids (2012), doi:10.1016/j.compfluid.2011.12.008

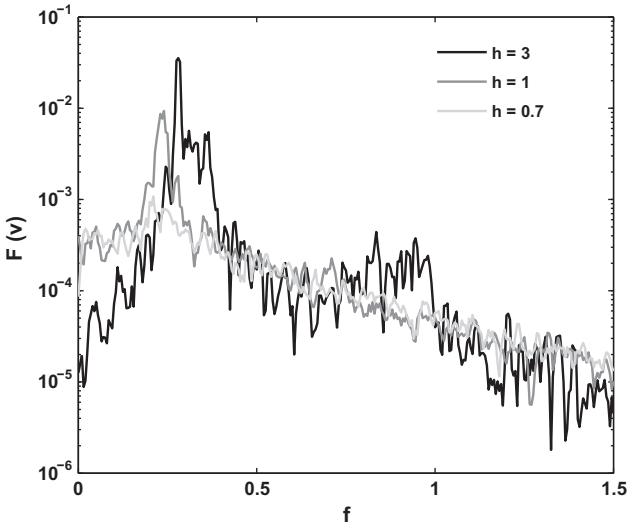

Fig. 4. Fourier spectra of the velocity crossflow component $v(x = 12.25, y = 0)$, for $h = 3$ (black line), $h = 1$ (dark gray) and $h = 0.7$ (light gray). The dominant frequency is decreasing with respect to confinement.

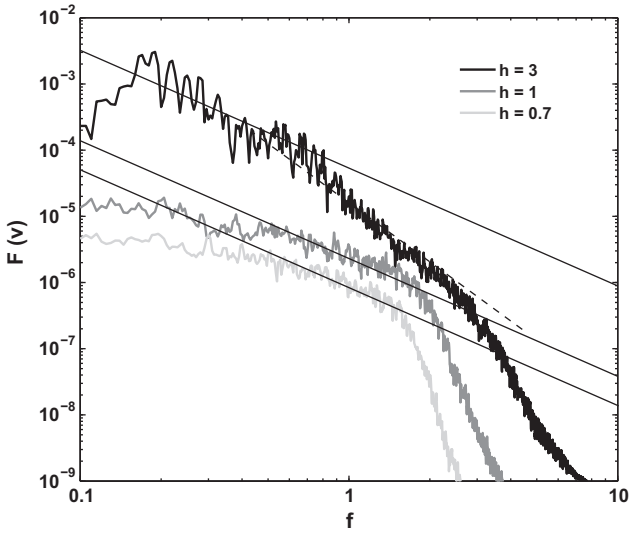

Fig. 5. Fourier spectra of the velocity crossflow component $v(x = 51.85, y = 0)$, for $h = 3$ (black line), $h = 1$ (dark gray) and $h = 0.7$ (light gray). Thin lines represent the slopes $-5/3$ (continuous) and -3 (dashed).

$$\sum_j (\nu\partial_j\partial_j u_i + \partial_j(\epsilon_j Q_j \partial_j u_i)) = \sum_j (\nu\partial_j(1 + \nu^{-1}\epsilon_j Q_j)\partial_j u_i)$$
$$= \sum_j \nu\partial_j \tilde{\partial}_j u_i \quad (9)$$

with $\tilde{\partial}_j = (1 + \nu^{-1}\epsilon_j Q_j)\partial_j$. (10)

Thus, using the SVV stabilization technique simply requires to set up SVV modified differential operators in the preprocessing phase of the computation. Consequently, there is no computational time overhead during the simulation.

Turbulent kinetic energy profiles and the corresponding dissipation rates are presented in the present paper. As well known, computations of the turbulent kinetic energy from LES simulations are generally satisfactory, because the energy associated to the small scale may be neglected. On the contrary, the computation of the corresponding dissipation rate would fail if a standard formulation was used, since in LES the dissipation does not result from viscous effects but from subgrid effects. This limitation may be overcome in the present SVV–LES approach, as explained in the appendix, and dissipation rates can be trustfully estimated.

Concerning the SVV parameters we proceed as suggested in Pasquetti [23], i.e. we try to decrease the SVV stabilizing terms. Our choice for the threshold frequency was $m_N = \sqrt{N}$, while $m_N = N/2$, which is, e.g. used in Karamanos and Karniadakis [14], was not found sufficiently stabilizing. For the amplitude we have used $\epsilon_N = 1/N$, except for $h = 1$ and FS conditions, where we used $\epsilon_N = 2/N$.

3. Confined turbulent wakes with no-slip conditions at the walls

In this section we investigate the influence of the confinement on several properties of the turbulence, at $Re = 5000$, using the inflow profile described in Section 2.1 and with NS conditions at the walls, $y = \pm(1 + h)$. Statistical quantities as mean velocity profiles, turbulent kinetic energy and dissipation rate have been calculated once the transient state due to the initial random perturbation has left the domain and the turbulent flow is fully developed, i.e. in practice for $100 < t \leqslant t_f$, where the final time of computations is generally $t_f = 400$. Simulations have been carried out on the NEC SX8 computer of the IDRIS center or on the cluster of the Mésocentre SIGAMM, located at the "Observatoire de la Côte Azur". On a NEC SX8 parallel–vectorial super computer, each simulation requires about 500 CPU hours.

Table 3
Reynolds and Strouhal numbers for the three confinements, using (i) the reference quantities introduced in the present study and (ii) those usually used for cylinder wakes.

h	Re	St	Re_c	St_c
3	5000	0.280	13695	0.409
1	5000	0.240	10000	0.480
0.7	5000	0.210	8696	0.483

3.1. Computational grid

Before going into the details of our results we give here some *a priori* and *a posteriori* justifications of our SVV–LES.

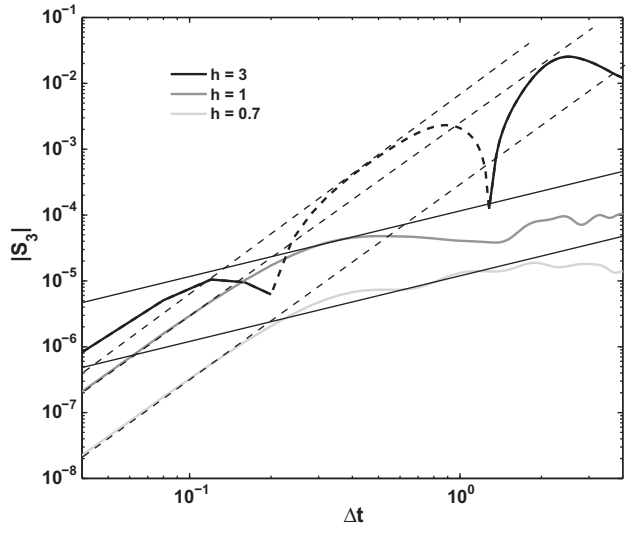

Fig. 6. Absolute value of the third order structure function S_3 versus time shift Δt for $v(x = 51.85, y = 0)$, for $h = 3$ (black line), $h = 1$ (dark gray) and $h = 0.7$ (light gray). Continuous lines depict negative values of S_3 and dashed lines depict positive values. Thin lines represent the slopes 1 (continuous) and 3 (dashed).

Please cite this article in press as: Biancofiore L et al. Influence of confinement on obstacle-free turbulent wakes. Comput Fluids (2012), doi:10.1016/j.compfluid.2011.12.008

We first use the fact that the considered grid is similar to the one required for DNS of the same flow but at the lower Reynolds number $Re = 500$, see Biancofiore et al. [5]. On the basis of Kolmogorov theory one can then deduce that a DNS, at $Re = 5000$, would require a refinement of the mesh in each spatial direction of $10^{3/4} \approx 5.62$. This fully justifies the use of LES: Such a rather poor refinement in each direction implies in the space–time domain a refinement of 10^3, and a much greater ratio in computational times, say at least 10^6. LES is thus required and moreover fully justified, because the value of 5.62 is sufficiently low to guarantee that the maximum frequency representable by the grid falls in the inertial range. Note that the present reasoning strongly relies on the use of a high order spectral method, so that numerical dissipation is negligible.

Another issue concerning LES is to know if "wall modeling" is required. In order to use some well established results, obtained from DNS or experiments, we consider the flow that will be recovered far downstream, i.e. the classical channel flow. To this end let us introduce the Reynolds number $\overline{Re}$ based on the flowrate velocity $\overline{U} = (h_1U_1 + h_2U_2)/(h_1 + h_2)$ and on the channel height $2(h_1 + h_2)$:

$$\overline{Re} = \frac{(U_1h_1 + U_2h_2)2}{\nu}. \tag{11}$$

One easily checks that:

$$\frac{\overline{Re}}{2Re} = 1 + \Lambda + h(1 - \Lambda). \tag{12}$$

In order to determine the friction Reynolds number $Re_\tau = (h_1 + h_2)/\delta_\nu$, where δ_ν is the viscous lengthscale, one uses the fact that a good approximation of Re_τ with respect to $\overline{Re}$ is $Re_\tau \approx 0.09\overline{Re}^{0.88}$, see Pope [27] and references herein. Table 1 shows, for the three considered values of $h = h_2/h_1$, the Reynolds numbers $\overline{Re}$ and Re_τ as well as the dimensionless distances δy and, in wall units, $\delta y^+ = Re_\tau \delta y/(1 + h)$, of the collocation point the nearest from the wall. For the three different values of h one observes that $\delta y^+ = O(1)$, so that a "near wall modeling" approach is not mandatory.

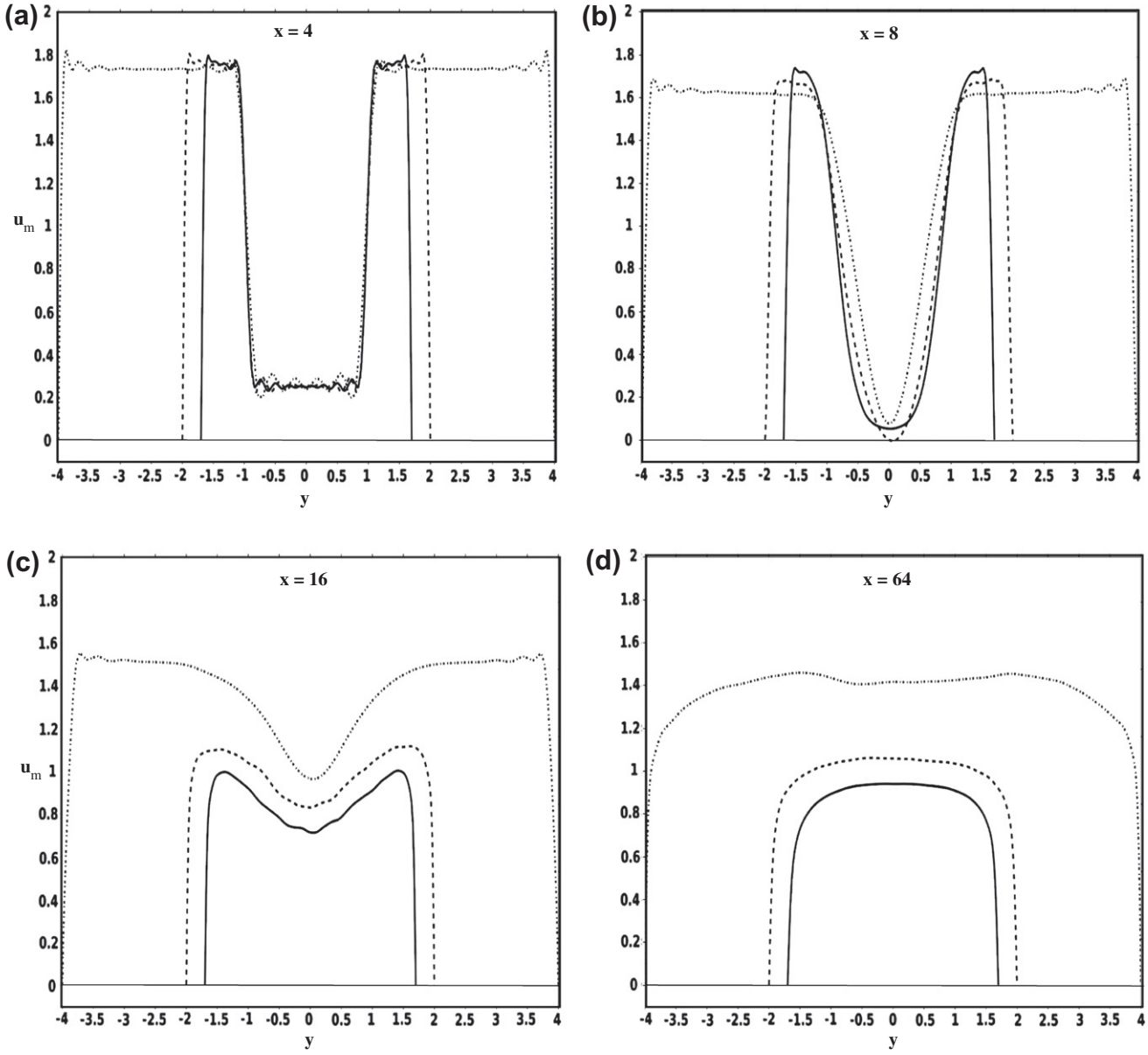

Fig. 7. Mean streamwise velocity profile $u_m(x, y)$ versus the crossflow direction y for $h = 3$ (dotted line), $h = 1$ (dashed line) and $h = 0.7$ (solid line), at different abscissa: (a) $x = 4$, (b) $x = 8$, (c) $x = 16$ and (d) $x = 64$.

Please cite this article in press as: Biancofiore L et al. Influence of confinement on obstacle-free turbulent wakes. Comput Fluids (2012), doi:10.1016/j.compfluid.2011.12.008

Since a spectral method is used, we can also check if the SVV stabilized flow is well resolved by our discretization. For the intermediate value $h = 1$, Fig. 2 shows the spectra of the instantaneous streamwise velocity at time $t = 400$, as computed along the x-streamwise, y-crossflow and z-spanwise axis issued from the points $(23.58, 0, 0)$ and $(51.58, 0, 0)$. In the y-direction, one has the absolute values of the coefficients $\hat{u}_k$ such that $u(x,y,z) = \sum_k \hat{u}_k(x,z) T_k \circ f^{-1}(y)$, where T_k is the Chebyshev polynomial of degree k and f the y-mapping from the reference to the physical domain, i.e. such that $f:[-1, 1] \to [-(1+h), 1+h]$. In x-direction, the definition is similar except that one considers only the subdomain that contains the point under consideration. In z-direction, it is the modulus of the Fourier spectrum which is visualized. As expected one observes an exponentially fast decay of the spectra, which means that the SVV stabilized Navier–Stokes equations are well resolved by the discretization. Similar results may be obtained at other test-points or for the transverse components of the velocity.

Since periodicity is assumed in the spanwise direction, it should be checked that the width $E = 8$ of the computational domain has been chosen sufficiently large. Two point-correlations of the transverse velocity components have been computed to this end. Table 2 shows, e.g. for the crossflow velocity, the ratio $\langle v(x,y,z)\, v(x,y,\ z+l)\rangle / \langle v(x,y,z)^2\rangle$, at the two points $(23.58, 0, 0)$ and $(51.58, 0, 0)$ for several values of l. Under the usual hypothesis of ergodicity, the statiscal means have been estimated by integration in time, in practice over the dimensionless time interval $(200, 400)$. These results have been obtained for the intermediate value $h = 1$. Despite the fact that the integration interval is relatively small one clearly observes a strong decrease of the considered two-point correlations.

3.2. Instantaneous flow field

We show in Fig. 3a–c the instantaneous modulus of the vorticity $|\boldsymbol{\omega}|$ in the (x, y) plane $z = 0$ at time $t = t_f = 400$ for the different confinement configurations ($h = 3$, $h = 1$ and $h = 0.7$). One observes that the position of the turbulent front depends on the confinement parameter, since it is located more upstream when the confinement is strengthened. While for $h = 1$ and $h = 0.7$ the flow seems to be fully 3D turbulent, for $h = 3$ the turbulence seems to be characterized by a peculiar two-/three-dimensional behaviour. This hypothesis is confirmed by Fig. 3d–f, where we show the instantaneous modulus of the vorticity in the (x, z) plane $y = 0$ at the same time $t = 400$. Looking at Fig. 3d it is clear that in the first part of the domain, i.e. for $x \lesssim 45$, the effect of the third dimension is negligible, which supports the conjecture of a two-dimensional turbulence in the considered region. Furthermore, in Fig. 3a the structures around the vortices upstream of the turbulent front suggest a direct cascade of enstrophy, which is characteristic of two-dimensional turbulence. Such structures are not detected for stronger confinements.

One may then think that confinement promotes a fully 3D turbulence. This hypothesis has however to be confirmed by a more detailed analysis.

3.3. Strouhal number

The Fourier analysis of temporal data at some measurement points allows the determination of the Strouhal number, in order to estimate the influence of the confinement on the dominant frequency. Let us remember first that for the wake of a cylinder the influence of confinement on the shedding frequency has already been investigated. Particularly, in experiments with a confined circular cylinder at Reynolds number such that $10^4 < Re < 10^7$, it is found that the Strouhal number increases when enforcing the confinement until $h = 1$ [30]. A similar tendency was found by Kim et al. [15], who compared $h = 4$ and $h = \infty$ results for LES of confined turbulent wakes past a square cylinder at $Re = 3000$. However, cylinder wakes are quite different from the obstacle-free wakes considered in our simulations, for which, up to our knowledge, no previous experiments or numerical simulations in the turbulent regime have been carried out. Moreover, as discussed later, the usual choice of the relevant reference quantities differs for these two different kinds of wake flows.

We show in Fig. 4 spectra of the velocity crossflow component v at $x = 12.25$, $y = 0$ for the examined confinements. The dimensionless frequency f is based on the reference value U_m/h_1. Since the flow is homogeneous in the transverse direction, the spectra are averaged over the z-points in order to improve the statistical sample. The main peak is damped when strengthening the confinement and the corresponding Strouhal number, St, decreases as the confinement is increased. Moreover, for $h = 3$ one observes a large band frequency peak around $f \approx 0.8$ which may reflect a backscattering phenomenon, e.g. typical of transitional turbulent shear flows, since at $x = 12.25$ the $h = 3$ flow is not yet fully developed, see Fig. 3.

At first sight the dependence of the Strouhal number on the confinement is opposite to the one observed for confined cylinder wakes. For cylinder wakes, Re and St are however generally based on the flowrate velocity $\overline{U}$ and the cylinder diameter $2h_1$, in contrast with our definition. To allow comparisons, the Reynolds and Strouhal number rescaled by means of these reference scales are named Re_c and St_c, respectively. One obtains:

$$\frac{Re_c}{2Re} = \frac{2St}{St_c} = \frac{1 + \Lambda + (1-\Lambda)h}{1+h} \tag{13}$$

Table 3 provides the values of Re, St, Re_c and St_c for the three different confinements. We notice that the variations of St and St_c are opposite, since St_c is decreasing with h, whereas St is increasing. Despite the fact that Re_c is decreased, so that one could imagine a decrease of St_c, see e.g. Williamson [34] for the wake of a cylinder, the increase of confinement induces a growth of St_c similar to cylinder wakes [30,15]. This tendency on St_c was already encountered by Biancofiore [3] for $Re = 100$, for the same value of the velocity ratio $\Lambda = -0.739$.

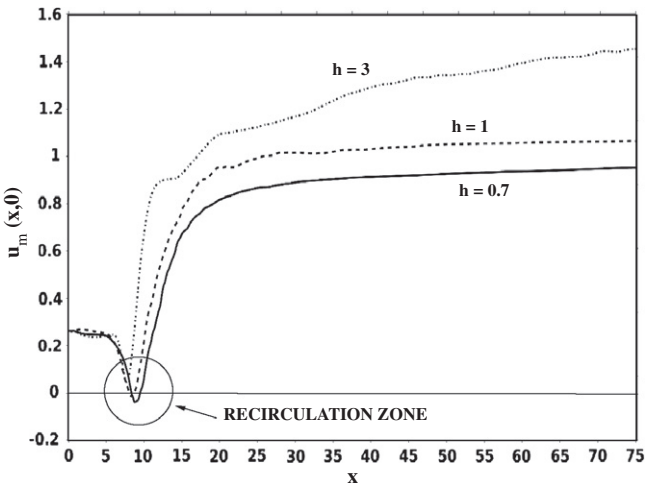

Fig. 8. Mean streamwise velocity $u_m(x, 0)$ versus the streamwise x-direction for $h = 3$ (dotted line), $h = 1$ (dashed line) and $h = 0.7$ (solid line). A recirculation region is only present for $h = 0.7$ and $h = 1$.

3.4. Velocity spectra and structure function

One-dimensional velocity spectra, based on the Fourier analysis of temporal data and obtained through the Taylor hypothesis, allow a comparison with the Kolmogorov spectrum typical of isotropic turbulent flows. In Fig. 5 one dimensional crossflow velocity spectra are presented (in log–log setting). The measurement point is located at $x = 51.85$, $y = 0$, i.e. beyond the 2D–3D transition for all the examined confinements. The most confined cases, i.e. $h = 1$ and $h = 0.7$, present a classical inertial subrange,

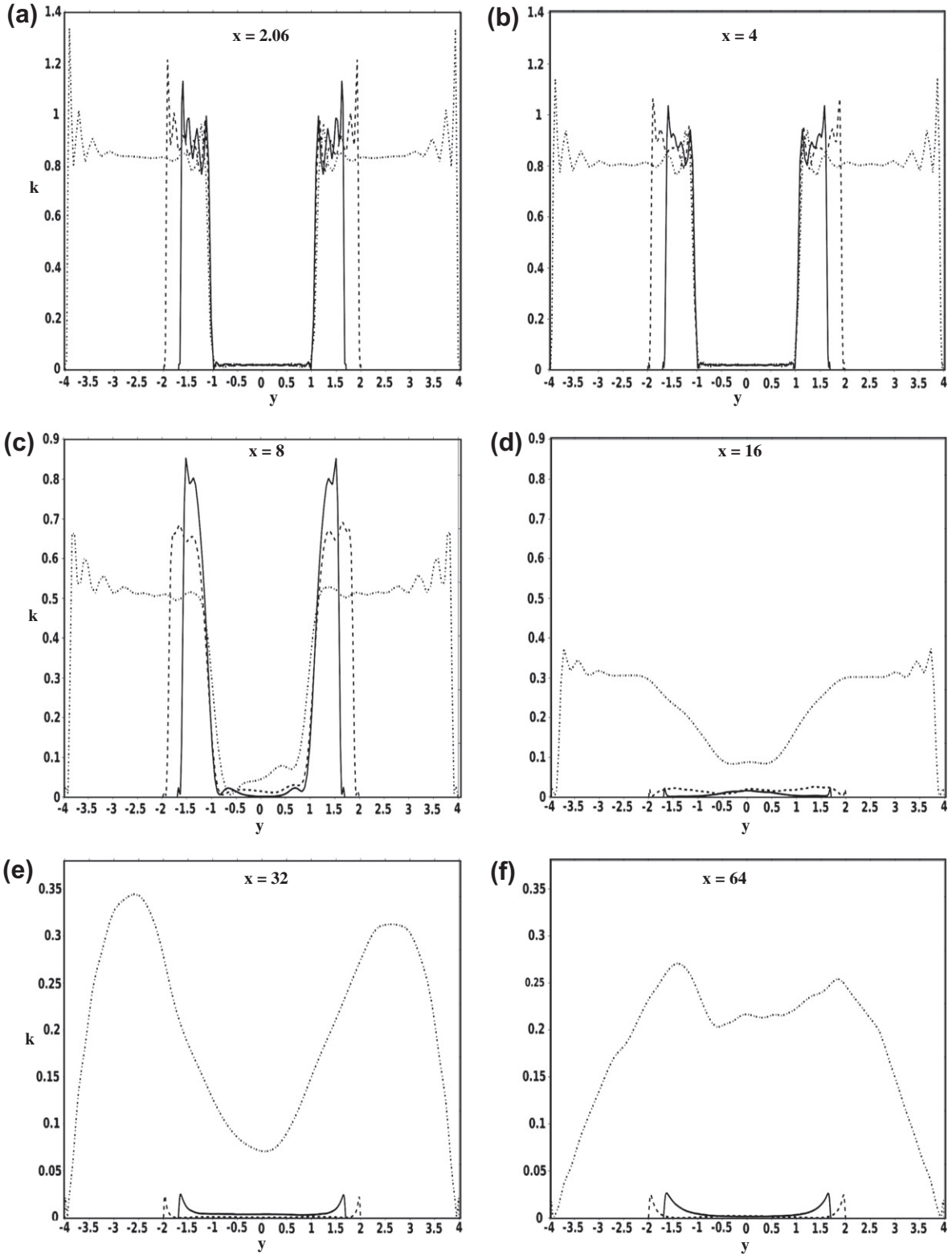

Fig. 9. Turbulent kinetic energy k versus crossflow y-direction for $h = 3$ (dotted line), $h = 1$ (dashed line) and $h = 0.7$ (solid line), at (a) $x = 2.04$, (b) $x = 4$, (c) $x = 8$, (d) $x = 16$, (e) $x = 32$ and (f) $x = 64$.

Please cite this article in press as: Biancofiore L et al. Influence of confinement on obstacle-free turbulent wakes. Comput Fluids (2012), doi:10.1016/j.compfluid.2011.12.008

where the Kolmogorov direct energy cascade takes place which is typical of a fully 3D turbulent flow. In the inertial subrange, the slopes of the spectra fit satisfactorily with the expected $-5/3$ value. Towards small scales, both curves show a subgrid regime analogous to the dissipative regime, predicted by Kolmogorov's hypothesis, see e.g. Pope [27]. In contrast to this behaviour, the spectrum of the less confined case, i.e. $h = 3$, presents two different tendencies in the inertial subrange, which is a reminiscence of the spectra of a two-dimensional turbulent flow [18]. In the large scale range, the spectrum has a slope close to $-5/3$, which means that a cascade of energy with a constant flux takes place. For smaller scales, the slope of the spectrum rather approximates the value -3, see e.g. Kraichnan [16,17]. Following Kraichnan and Montgomery [18], this behaviour of the spectrum is typical of an inverse cascade of enstrophy, further hint of the 2D nature of the turbulence for $h = 3$.

In order to confirm this hypothesis, one can compute the third order-velocity structure function of the velocity $S_3(\mathbf{l}) = \langle[(\mathbf{u}(\mathbf{x}+\mathbf{l},t)-\mathbf{u}(\mathbf{x},t))\cdot\mathbf{l}/|\mathbf{l}|]^3\rangle$, which can distinguish between 2D and 3D turbulent flows [2]. In streamwise direction, by means of Taylor's

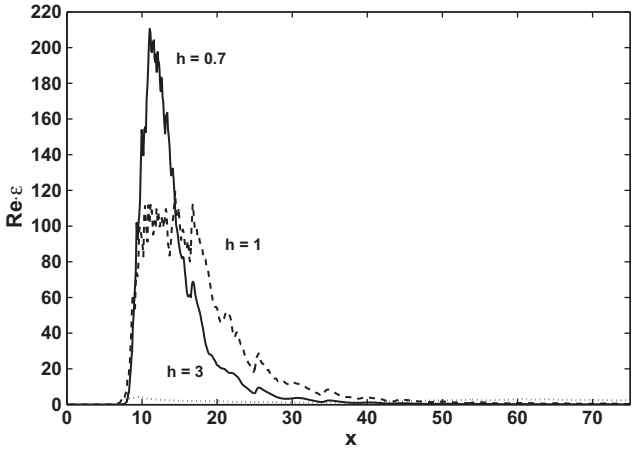

Fig. 11. Dissipation rate of turbulent kinetic energy times Re versus streamwise x-direction $y = z = 0$, for $h = 3$ (dotted line), $h = 1$ (dashed line) and $h = 0.7$ (solid line).

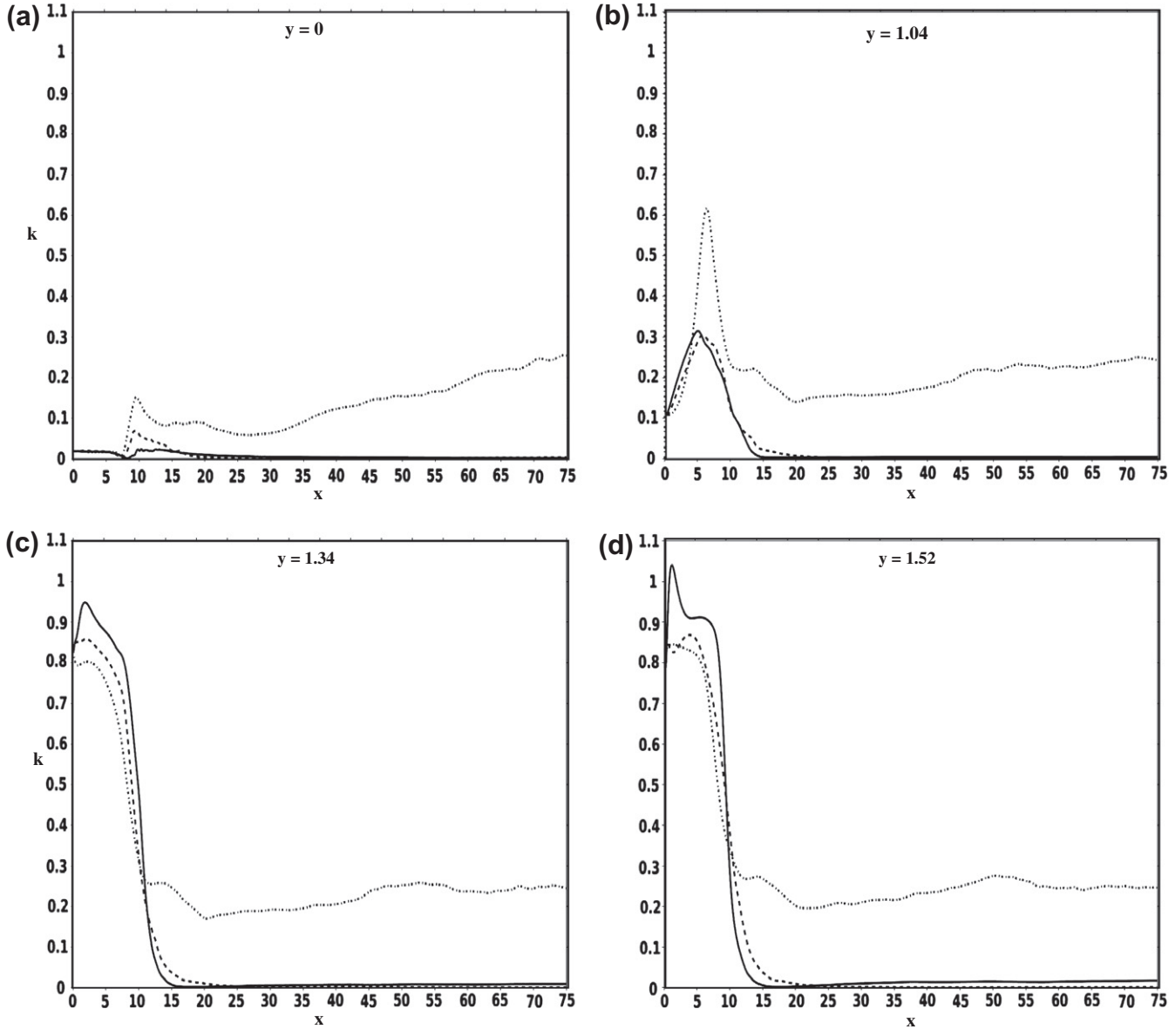

Fig. 10. Turbulent kinetic energy k versus streamwise x-direction for $h = 3$ (dotted line), $h = 1$ (dashed line) and $h = 0.7$ (solid line), at (a) $y = 0$, (b) $y = 1.04$, (c) $y = 1.34$ and (d) $y = 1.52$.

Please cite this article in press as: Biancofiore L et al. Influence of confinement on obstacle-free turbulent wakes. Comput Fluids (2012), doi:10.1016/j.compfluid.2011.12.008

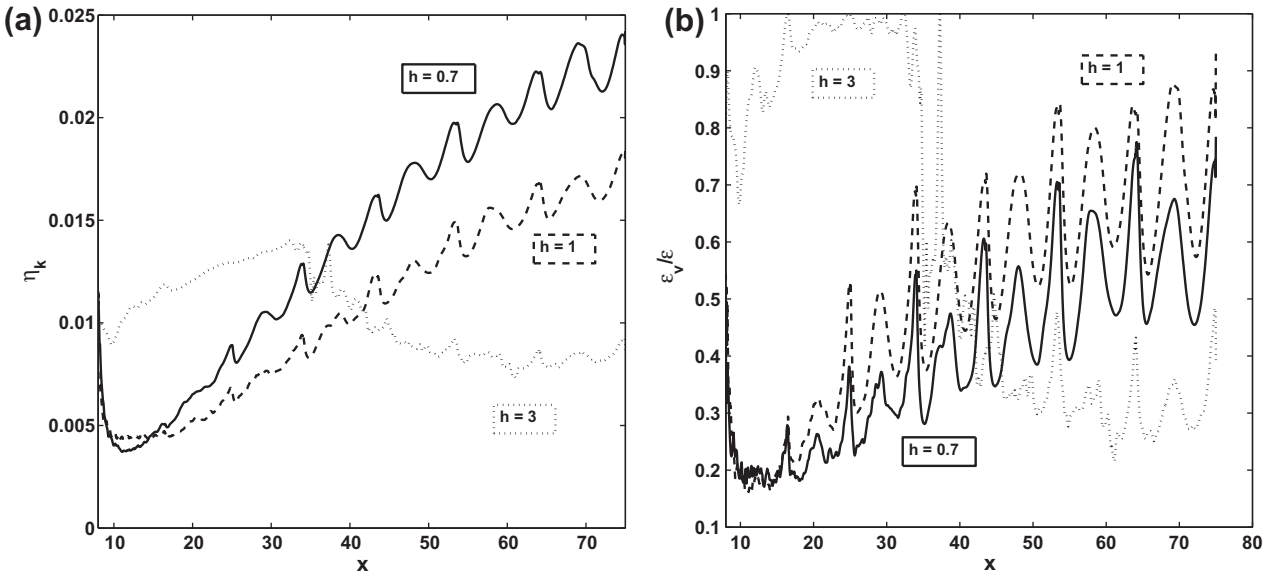

Fig. 12. (a) Kolmogorov scale and (b) ratio between physical and total dissipation rates versus streamwise x-direction $y = z = 0$, for $h = 3$ (dotted line), $h = 1$ (dashed line) and $h = 0.7$ (solid line).

hypothesis the third order structure function may be computed as a function of the time shift Δt, $S_3(\Delta t) = \langle [u(\mathbf{x}, t + \Delta t) - u(\mathbf{x}, t)]^3 \rangle$, at the same point ($x = 51.85$ and $y = 0$) and still averaging over the z-points. In an homogeneous and isotropic turbulent flow, the sign of the third order-velocity structure function can determine the direction of the energy cascade. If it is negative, there is a transfer of turbulent kinetic energy from the large scales towards the small scales, sign of a fully 3D turbulence. Otherwise, if it is positive the energy is transferred from the small scales towards the large ones, peculiar to a two-dimensional turbulent flow. Both inverse and direct cascade of energy have a slope of $S_3(\Delta t)$ equal to 1 [2]. For 2D turbulence, in Bernard [2] it is also shown that in the range, where the direct enstrophy cascade takes place, the third order-velocity structure function $S_3(\Delta t)$ is still positive and its slope (in log-scale) fits 3. This behaviour was confirmed by Lindborg [19] in atmospheric turbulence and recently by Boffetta and Musacchio [6] for forced 2D Navier–Stokes equations. Furthermore, in the subgrid regime the behaviour of $|S_3|$ approximates the theoretical slope of 3 for both 2D- and 3D-turbulence Bernard [2].

In Fig. 6, the behaviour of the absolute value $|S_3(\Delta t)|$ is reported for the three confinement configurations. Continuous lines mean negative values of S_3, while dashed lines mean positive ones. The slopes of 1 and 3 are depicted by continuous and dashed lines, respectively. One can note that for $h = 1$ and $h = 0.7$ the third order structure function is still negative, according to the hypothesis of a fully 3D turbulent flow, while for $h = 3$, a region for which S_3 is positive is encountered. Considering that our turbulent wakes do not respect the conditions of homogeneity and isotropy, we can conclude that the theoretical slopes are well recovered by the variations of S_3. In particular, while in the subgrid ranges the three configurations have a similar slope of 3, in the inertial range the behaviours differ. The fully 3D turbulent cases present a clear slope of 1, which represents the energy cascade, while for $h = 3$, the slope of S_3 is close to 3, sign of an enstrophy cascade. However, for $h = 3$ the presence of a range with positive values of $S_3(\Delta t)$ confirms the hypothesis of 2D turbulence. Furthermore, if one associates f to $1/\Delta t$, the positive range of the third order-velocity structure function corresponds roughly to the inertial subrange, where the direct cascade of enstrophy takes place, see Fig. 5. Thus, the behaviours of both the spectra and the third order-velocity structure function suggest that a stronger confinement favors the formation of fully 3D turbulent flow.

3.5. Mean flow and turbulence statistics

In this section statistical quantities characteristic of turbulence are analyzed. These quantities are averaged in time but also over the periodic spanwise direction, except for the dissipation rates which are computed in the plane $z = 0$.

3.5.1. Mean flow profiles

Fig. 7 presents profiles of the streamwise component of the mean flow velocity $u_m(x, y)$ at (a) $x = 4$, (b) $x = 8$, (c) $x = 16$, and (d) $x = 64$. From now, the dotted line depicts $h = 3$, the dashed one $h = 1$ and the continuous one $h = 0.7$. For $x = 64$, i.e. close to the computational domain outlet, the profiles are close to a "plug flow", especially for the strongest confinements. Asymptotically, each of the three flows will of course reach a fully developed state of turbulent channel flow.

Although the inlet profiles are co-flow wakes, for $h = 1$ the velocity is negative at the centerline, see Fig. 7b. In order to measure the length of the recirculation region and to reveal its existence for other confinements, Fig. 8 provides the mean streamwise velocity $u_m(x, 0)$ along the centerline. One notes that the weakest analyzed confinement $h = 3$ presents no recirculation zone, in contrast to $h = 1$ and $h = 0.7$. Moreover, the largest recirculation region is obtained for $h = 0.7$. Thus, the confinement promotes the formation of a mean recirculation bubble in the domain. This phenomenon is discussed in Biancofiore et al. [5] and our explanation is based on an asymmetric diffusion of the shear layer in the outer and inner wake regions. One may think that such an explanation could still hold by substituting a turbulent viscosity effect to the molecular viscosity effect.

3.5.2. Turbulent kinetic energy

The behaviour of the turbulent front observed in Fig. 3 may be interpreted as a destabilizing effect due to confinement. In order to confirm this intuition, the turbulent kinetic energy profiles should be analyzed. Fig. 9 illustrates the behaviour of the turbulent kinetic energy k as a function of the crossflow direction at six different

Please cite this article in press as: Biancofiore L et al. Influence of confinement on obstacle-free turbulent wakes. Comput Fluids (2012), doi:10.1016/j.compfluid.2011.12.008

abscissa, from $x = 2.06$ to $x = 64$. Note that the scale is changed between the different figures. Although not fully converged, as pointed out by the oscillations of the curves, such profiles allow a good evaluation of the variations of k. The symmetries that can be observed in Fig. 9a–c simply result from the fact that no perturbations are added to the inlet flow.

Close to the inlet, see Fig. 9a and b, the turbulent kinetic energy is larger than it is downstream and the maxima around $y = \pm 1$ have similar values independently of the confinement. Instead, for $x = 8$ (Fig. 9c), the highest peaks are those of strongest confinements, a further hint of a growth of the turbulence intensity associated to an increasing confinement. However, downstream the most confined flows loose a large part of their kinetic energy, see Fig. 9e-f. Thus, in the final part of the domain the turbulent character is higher for $h = 3$, as already noticed in the snapshots of Fig. 3 or in the spectra of Fig. 5.

Same conclusions can be drawn when analyzing Fig. 10, which illustrates the behaviour of the turbulent kinetic energy k along the streamwise direction, for (a) $y = 0$, (b) $y = 1.04$, (c) $y = 1.34$, and (d) $y = 1.52$. At $y = 0$, see Fig. 10a, the case with $h = 3$ presents the highest turbulent kinetic energy, but k at the centerline is negligible compared to its values closer to the boundaries. For $y = 1.34$ and $y = 1.52$, the configurations with the strongest confinement present the highest maxima, which means that the confinement enhances the turbulent character of the flow. This destabilizing influence is however only noticed close to the entry. Note that for $h = 0.7$, we have $y \leqslant 1.7$, so that the corresponding profile at $y = 1.52$ is not strongly affected by the boundary layer.

Downstream the least confined case presents the highest level of turbulence intensity. One may think that the boundary layers dissipate rapidly the turbulent kinetic energy, so that the least confined wake flow is the most turbulent in the final part of the domain. One may also conjecture that (i) once the turbulent wake flow has become similar to a standard turbulent channel flow, the velocity fluctuations are much less important and (ii) that this occurs farther downstream for the least confined flow. Finally, it is clear that the mean flow velocity and the width of the channel increase with h, so that a Reynolds number based on these quantities is higher for the least confined flow, see Table 1.

3.5.3. Dissipation rate

By means of Eq. (20), one can estimate the dissipation rate ε of the turbulent kinetic energy in order to study the connection of this quantity with the confinement. Fig. 11 shows the behaviour

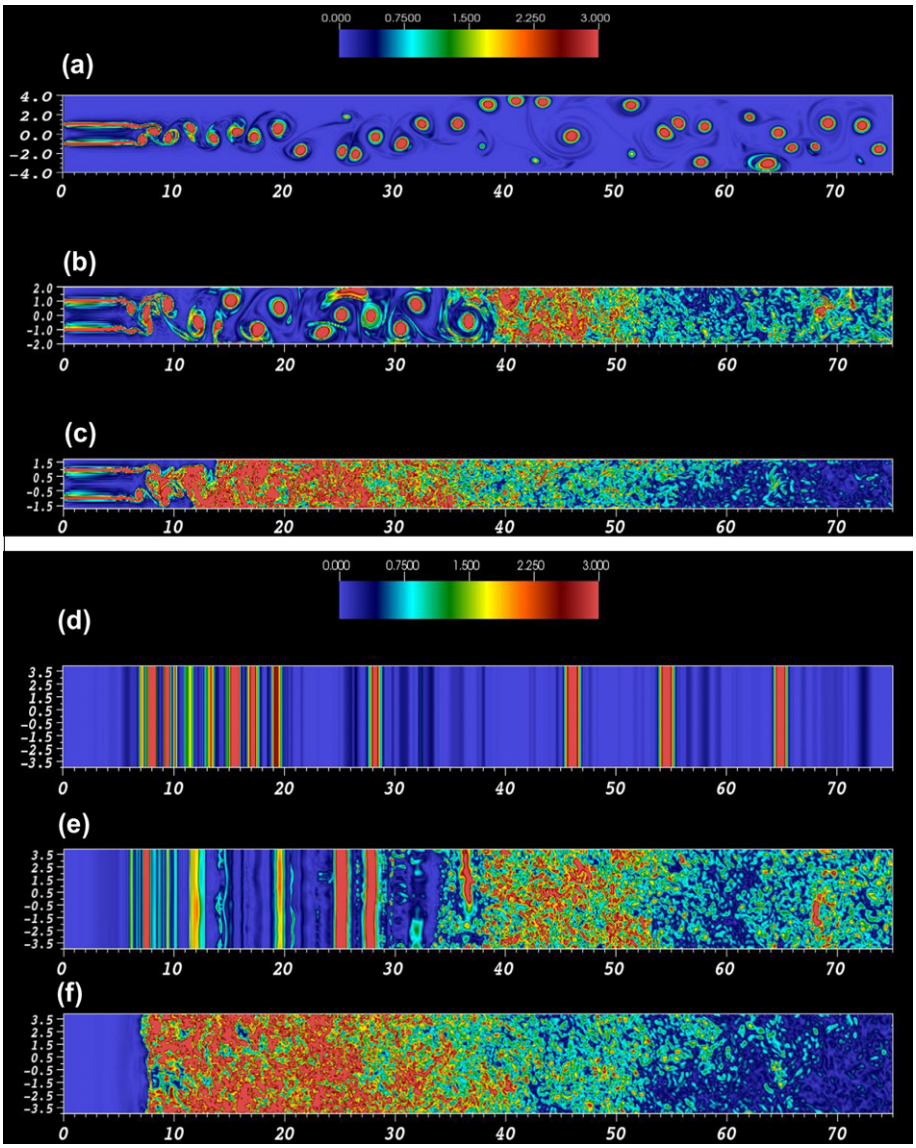

Fig. 13. Instantaneous modulus of the vorticity $|\omega|$ in the central planes $z = 0$ (top) and $y = 0$ (bottom) at $t = 400$ for FS-flows: (a, d) $h = 3$, (b, e) $h = 1$ and (c, f) $h = 0.7$.

Please cite this article in press as: Biancofiore L et al. Influence of confinement on obstacle-free turbulent wakes. Comput Fluids (2012), doi:10.1016/j.compfluid.2011.12.008

of $Re\ \varepsilon$ along the centerline $y = z = 0$. One observes that the maximum of dissipation rate ε is enhanced when the confinement is increased. Another effect should be noticed: while for the two strongest confinements a large part of the dissipation occurs close to the inlet, for $h = 3$ the dissipation persists along the domain. One may think that the explanations provided for the turbulent kinetic energy also hold for the dissipation rates.

By means of the dissipation rate ε, one can try to provide some additional *a posteriori* justifications to our LES calculations. In particular, we can estimate the Kolmogorov scale $\eta_K = Re^{-3/4}\ \varepsilon^{1/4}$. It is also possible to provide the ratio between the dissipation rate ε_v, only associated to the dimensionless viscosity (Re^{-1}), to the dissipation rate ε, which takes into account both the physical and subgrid dissipation terms, see the Appendix for details. Fig. 12 shows these quantities along the centerline $y = z = 0$. The most turbulent configurations, i.e. $h = 0.7$ and $h = 1$, present a minimal Kolmogorov scale $\eta_K \approx 4 \times 10^{-3}$ for $x \approx 12$, while for $h = 3$ the minimum is $\eta_K \approx 7 \times 10^{-3}$ for $x \approx 60$, see Fig. 12a. Such estimates confirm that LES was required, since the average grid sizes along the streamwise direction that correspond to the minima are $\Delta x = 0.085$ and $\Delta x = 0.011$ for $h = \{0.7,1\}$ and $h = 3$, respectively. Similar conclusions can be drawn when observing the behaviour of the ratio $\varepsilon_v/\varepsilon$ along the x-direction. The minima are $\varepsilon_v/\varepsilon \approx 0.18$ and $\varepsilon_v/\varepsilon \approx 0.21$ for $h = \{0.7,1\}$ and $h = 3$, respectively. These estimates show that our LES do not simply rely on the subgrid dissipation and so give some confidence in the numerical results. They agree with those generally encountered in SVV–LES of turbulent flows at comparable Reynolds numbers [25].

4. Confined turbulent wakes with free slip conditions at the walls

The formation of boundary layers due to the NS conditions is one of the main physical mechanisms that could explain the enhancement of the turbulent character of the flow as the confinement is increased. In the presence of confinement, the boundary layers start to interact with the shear layers located around $y = \pm 1$. In this section, we therefore analyze a FS condition at the wall, in order to study the direct influence of confinement on the turbulent wakes.

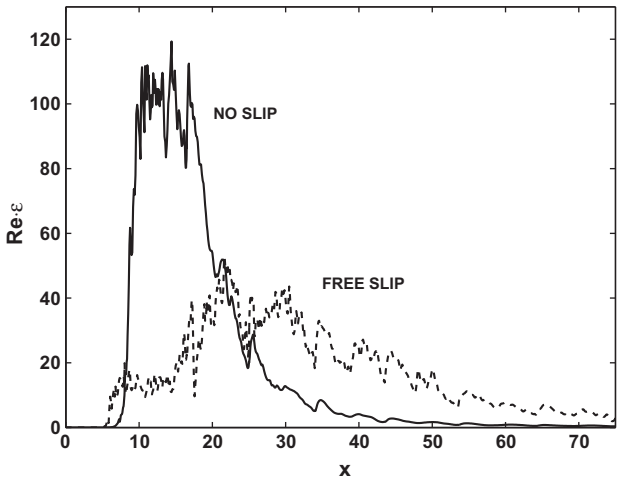

Fig. 15. Dissipation rate of turbulent kinetic energy ε times Re versus streamwise x-direction $y = z = 0$ for $h = 1$. The continuous line depicts NS conditions and the dashed one FS conditions.

For the three different values of the confinement parameter ($h = 3$, $h = 1$ and $h = 0.7$), Fig. 13 illustrates the instantaneous modulus $|\boldsymbol{\omega}|$ of vorticity at time $t = 400$ in the (x, y) plane $z = 0$ (a–c) and (x, z) plane $y = 0$ (d–f). Comparing with NS-flows, see Fig. 3, we can note that for each configuration the NS conditions enhance the 3D character of the turbulence. Thus, for $h = 1$ the turbulent front is moved downstream and for the weakest confinement, $h = 3$, no clear turbulent front is detected and the flow seems to be 2D laminar or only characterized by two-dimensional turbulence. However, even without boundary layer the confinement clearly promotes a fully three-dimensional turbulence. The analyzes of the one-dimensional velocity spectra and of the third-order structure function are carried out for $h = 3$ in Section 5.

Fig. 14 shows the behaviour of the turbulent kinetic energy in the streamwise direction at (a) $y = 1.34$ and (b) $y = 1.52$ for FS-flows. The growth of the turbulent kinetic energy with respect to confinement is also clear in that case.

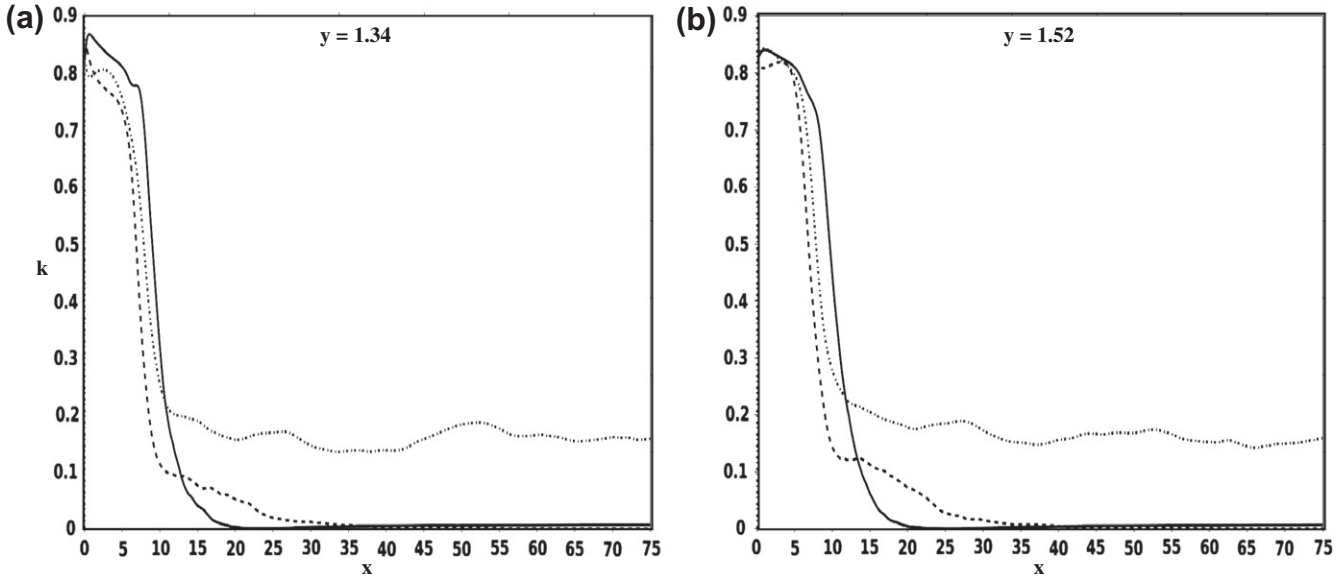

Fig. 14. Turbulent kinetic energy for the FS-flows with respect to streamwise direction x at (a) $y = 1.34$ and (b) $y = 1.52$, for $h = 3$ (dotted line), $h = 1$ (dashed line) and $h = 0.7$ (solid line).

Please cite this article in press as: Biancofiore L et al. Influence of confinement on obstacle-free turbulent wakes. Comput Fluids (2012), doi:10.1016/j.compfluid.2011.12.008

In Fig. 15 we compare the dissipation rates ε, as computed with Eq. (20), of FS- and NS-flows for the confinement parameter $h = 1$. Clearly, the dissipation is stronger with NS conditions than with FS conditions. The comparison between FS- and NS-flows suggests the role of the boundary layers at the walls. The presence of boundary layers enhances the 3D turbulent nature of the flows (see Section 5

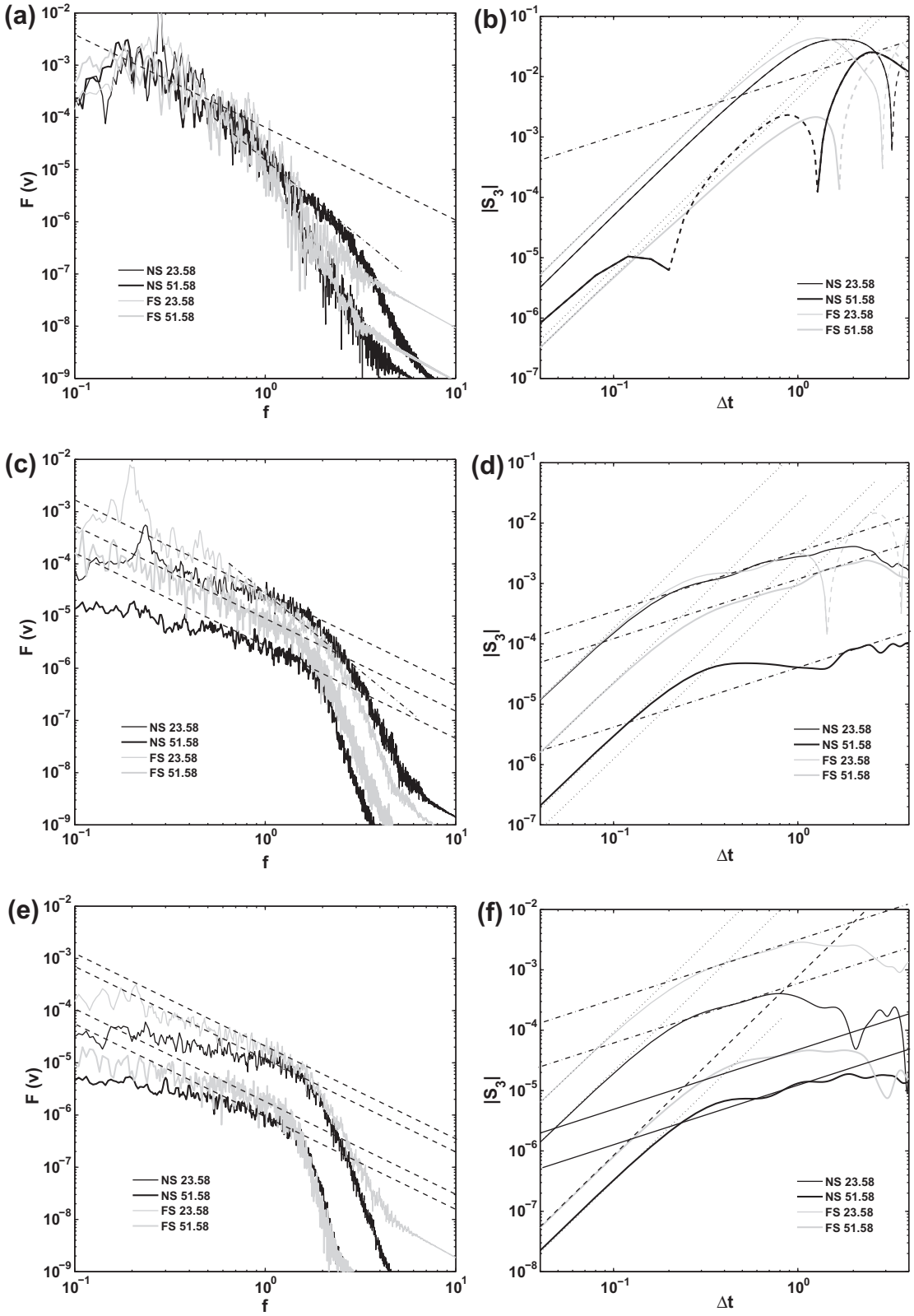

Fig. 16. (a, c, e) One-dimensional velocity spectra and (b, d, f) absolute value of the third order structure function S_3 versus time shift with (a, b) $h = 3$, (c, d) $h = 1$ and (e, f) $h = 0.7$. The two quantities are measured at two different abscissa $x = 23.58$, and $x = 51.58$, depicted by thin and bold lines, respectively (black: NS, gray: FS). In (a, c, e) dashed and dash-and-dot lines represent the slopes $-5/3$ and -3, respectively. In (b, d, f) continuous lines depict negative values of S_3 and dashed lines depict positive values. Dash-and-dot and dotted lines represent the slopes of 1 and 3, respectively.

Please cite this article in press as: Biancofiore L et al. Influence of confinement on obstacle-free turbulent wakes. Comput Fluids (2012), doi:10.1016/j.compfluid.2011.12.008

for a detailed analysis on this aspect) and, subsequently, their interactions with the shear layers still increase the development of the turbulence. However, the role of the boundary layers cannot explain alone the growth of the turbulent kinetic energy due to the confinement, since for FS-flows the turbulent character of the wakes is also enhanced by confinement. Biancofiore [3] noticed in contrast that for lower Reynolds number, i.e. $Re = 100$ and $Re = 500$, NS conditions were stabilizing by lowering the critical co-flow parameter required for onset of instability. When boundary layers develop, a significant difference is hence noticed between laminar and turbulent wake flows.

5. 2D versus 3D turbulence

In this section a comparison for both boundary conditions between the 2D/3D character of the turbulence is illustrated by means of two different analyzes: the third-order velocity structure function (Section 5.1) and the Lumley's diagram (Section 5.2).

5.1. Third-order velocity structure function

In Fig. 16a–e we illustrate the behaviour of the velocity spectra and in Fig. 16b–f the absolute value of the third order structure function for both NS- and FS-flows. This is done at two different abscissa, $x = 23.58$ and $x = 51.58$, and for the three different confinements (a, b) $h = 3$, (c, d) $h = 1$ and (e, f) $h = 0.7$.

For $h = 3$ (Fig. 16a and b) and $x = 23.58$, i.e. close to the inlet, the spectra and the structure functions of the NS- and FS-flows are very similar, sign that the effect of boundary layers is not yet relevant. In particular, only the largest scales are characterized by a positive third order-velocity structure function. Moreover, the spectra do not show a direct cascade of enstrophy. Also at medium scales it seems that a dissipative subrange is already present and thus, that the effect of viscosity is not negligible, which is peculiar to laminar flows. However, at $x = 51.58$ the NS-flow shows both a two- and three-dimensional turbulent character, as already described in Section 3.4, while for the FS-flow the laminar nature seems to persist.

For $h = 1$ (Fig. 16c and d), at both abscissa the flows present a fully 3D turbulent nature. However, for FS-flows and close to the inlet, an enstrophy cascade occurs, sign of a two-dimensional turbulence. This fact is confirmed also by the positive range of the third order structure function, see Fig. 16d. The 2D turbulent character is lost downwards, as illustrated by the spectrum and the structure function at $x = 51.58$. In this case, the spectrum only presents a direct energy cascade (slope $-5/3$) and the structure function is always negative. However, because the flows are far from the conditions of isotropy and homogeneity, a perfect agreement

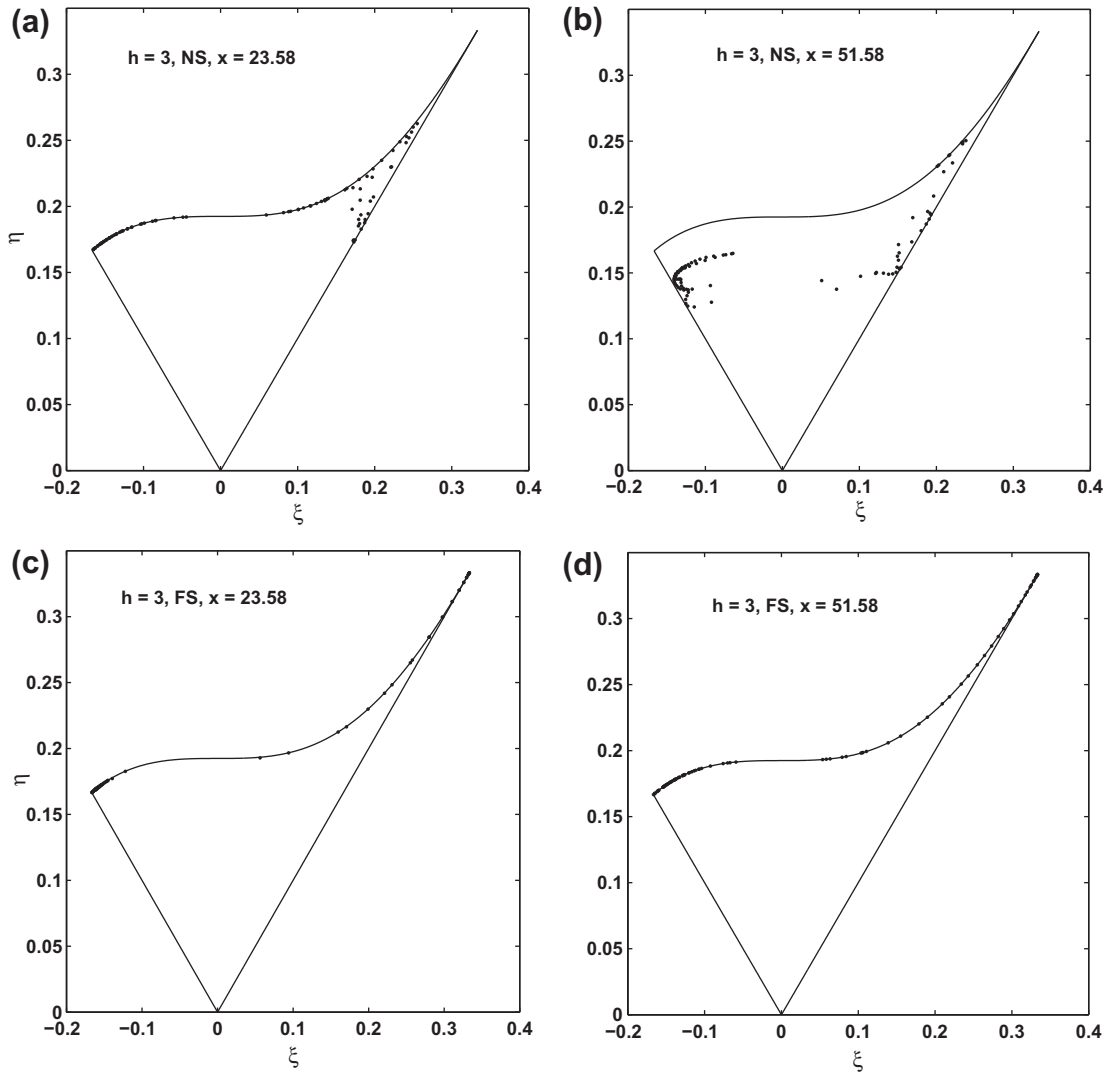

Fig. 17. Sketch of anisotropy tensor in the Lumley triangle for $h = 3$ and (a) NS, $x = 23.58$, (b) NS, $x = 51.58$, (c) FS, $x = 23.58$ and (d) FS, $x = 51.58$.

Please cite this article in press as: Biancofiore L et al. Influence of confinement on obstacle-free turbulent wakes. Comput Fluids (2012), doi:10.1016/j.compfluid.2011.12.008

of the curves of $S_3(\Delta t)$ in the inertial subrange with the slope of 1 cannot be expected, especially for cases, where a change of sign occurs.

Same results are shown for $h = 0.7$ in Fig. 16e and f. In this case, for both NS- and FS-flows and both abscissa, the turbulence is only characterized by 3D features. No cascade of enstrophy is detected and moreover S_3 is always negative.

In conclusion, the interaction between the wake and the vorticity created at the boundaries seems to have a relevant role in the formation of turbulence, both in 2D and 3D regimes. Thus, in the first part of the channel the FS- and NS-flows have a similar laminar behaviour for $h = 3$, but when the boundary layers start to interact with the wake, 2D and 3D turbulent features are only detected for NS-flows.

Another way to investigate the 2D/ 3D nature of turbulence is provided by Lumley diagrams, which are based on a fine analysis of the Reynolds stress tensor, see Section 5.2.

5.2. Lumley's diagrams

In order to analyze the anisotropy features of the turbulence for the examined wakes, we provide in Figs. 17–19 Lumley's diagrams [20] for $h = 3$, $h = 1$ and $h = 0.7$ respectively. Each diagram corresponds to a given streamwise x-value and each point to a y-crossflow value (averaging is done both in time and in z-direction). For all the three figures, (a) and (b) illustrate Lumley's diagrams at $x = 23.58$ and $x = 51.58$ with NS conditions, while (c) and (d) show such diagrams at the same abscissa but with FS conditions. The anisotropy tensor is defined as the deviatoric part of the Reynolds stress tensor normalized by its trace, i.e. by the double of the turbulent kinetic energy. One observes that for each configuration, the points associated to the non null invariants (ξ, η) of the anisotropy tensor remain within the region delimited by the three solid lines. This points out that our LES results respect the realizability diagram of Lumley [20,27].

In Fig. 17a, c, and d, the presence of (ξ, η) points on the upper side of the "triangle" means a two-component anisotropy. In particular, in figures c and d, all samples collapse on the upper side of the triangle. This behaviour of the invariants agrees with the results obtained in Section 5.1 which have pointed out the presence of two-dimensional laminar/ turbulent structures for these configurations. In absence of boundary layers (figures c and d) the three-dimensional character completely disappears. Conversely, a large part of the two-dimensional behaviour is lost for $x = 51.58$, see Fig. 17b. Same results were obtained by analyzing the spectra and structure functions in Fig. 16a and b.

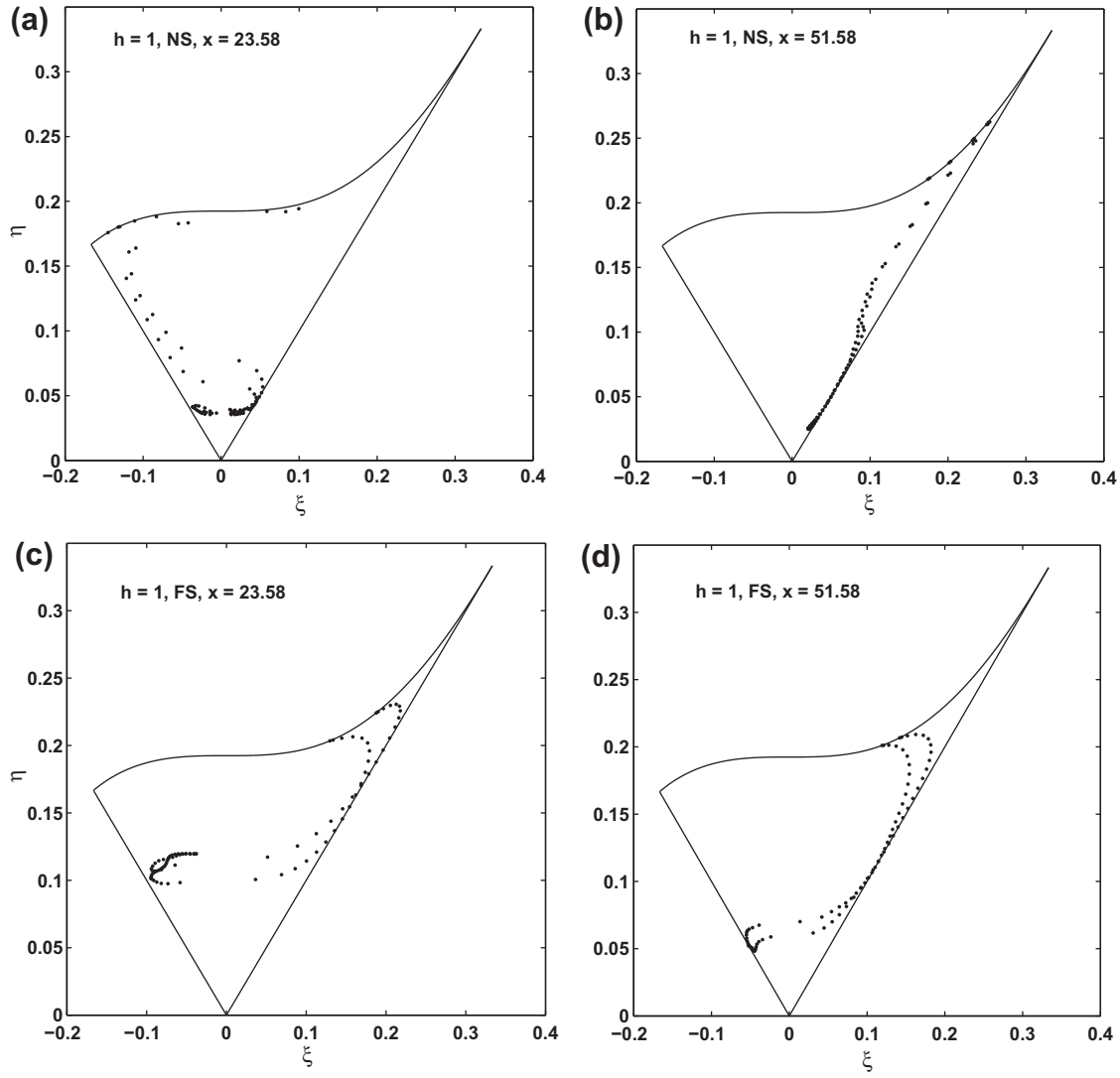

Fig. 18. Sketch of anisotropy tensor in the Lumley triangle for $h = 1$ and (a) NS, $x = 23.58$, (b) NS, $x = 51.58$, (c) FS, $x = 23.58$ and (d) FS, $x = 51.58$.

Please cite this article in press as: Biancofiore L et al. Influence of confinement on obstacle-free turbulent wakes. Comput Fluids (2012), doi:10.1016/j.compfluid.2011.12.008

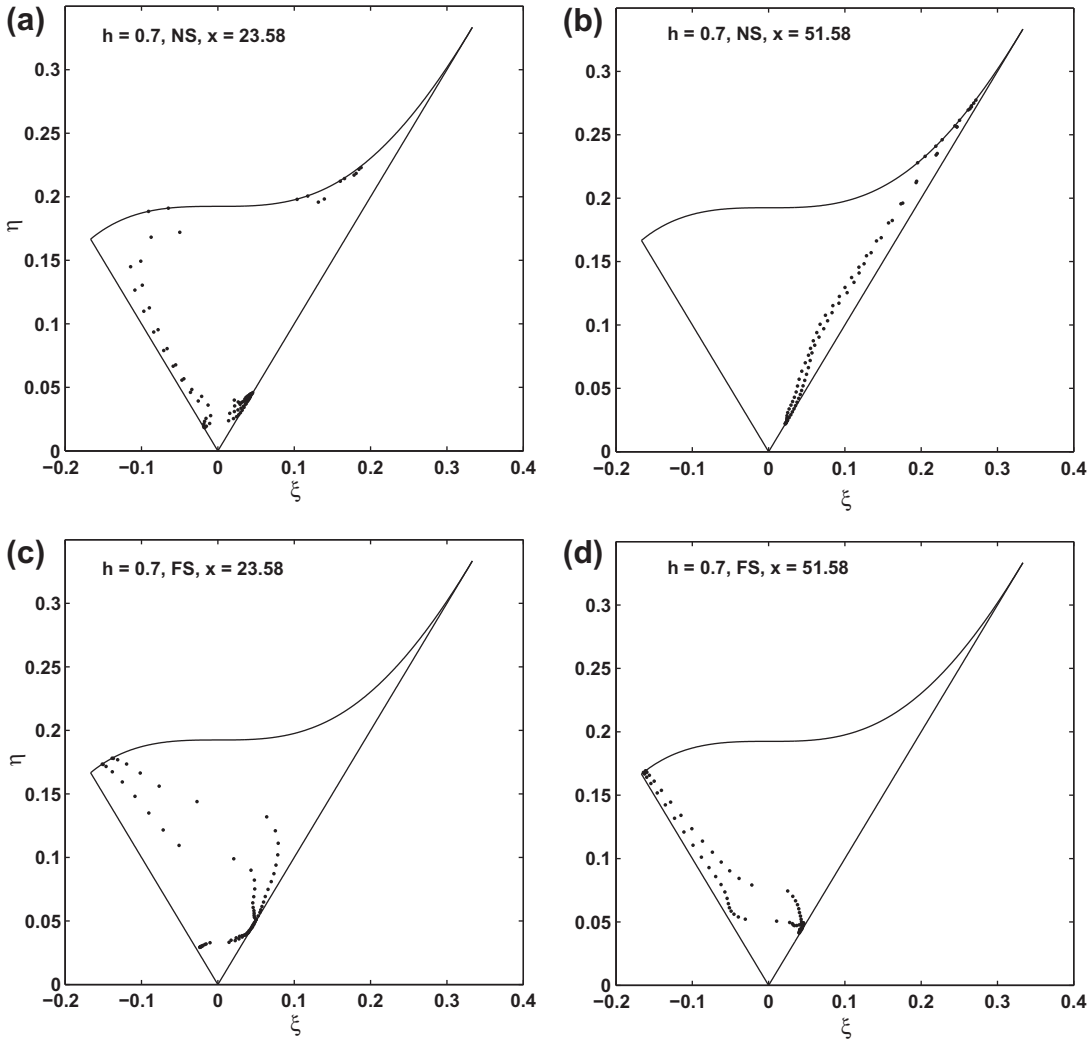

Fig. 19. Sketch of anisotropy tensor in the Lumley triangle for $h = 0.7$ and (a) NS, $x = 23.58$, (b) NS, $x = 51.58$, (c) FS, $x = 23.58$ and (d) FS, $x = 51.58$.

In Fig. 18a, the distribution of the (ξ, η) points reminds a turbulent mixing layer, since in the bulk of such flow the Reynolds stresses are close to axisymmetric with positive ξ, while at its edges they are still axisymmetric but with negative ξ. This points out the dominance of the shear layers of the wakes in this region. Furthermore, the accumulation of points at the $(\xi = \eta = 0)$ vertex indicates a tendency towards an isotropic turbulence. Downwards, see Fig. 18b, the (ξ, η) point distribution is very similar to a turbulent channel flow, sign of the disappearance of the shear layers in the final part of the domain, see Fig. 7d. For FS conditions, the configuration is less obvious. However, at both abscissa the turbulence seems to be axisymmetric anisotropic, with positive/negative ξ depending on the distance of the considered point to the shear layers.

Finally, Fig. 19 shows that for NS flows the behaviour of the invariants for $h = 0.7$ is similar to the one obtained with $h = 1$. For FS flows, the configurations differ. The turbulence remains however axisymmetric but now rather characterized by negative ξ.

6. Conclusions and perspectives

In order to better understand the physical mechanism which takes place in the recessed injectors of rockets engines, we have carried out an academical study on the spatio-temporal development of 3D confined wakes. By means of high order LES based on a SVV technique (SVV–LES Chebyshev–Fourier spectral code) we have studied the influence of confinement on turbulent obstacle-free wakes. Considering several quantities like one-dimensional spectra, third-order velocity structure function, turbulent kinetic energy and dissipation rate, we have shown that confinement enhances the turbulent character of the flow. This is especially pointed out by the increase of turbulent kinetic energy and dissipation rate when the confinement is increased.

Comparing FS- and NS-flows, we have noticed that the presence of boundary layers increases the intensity of the turbulence and consequently the dissipation rate. This is an opposite effect to the one observed for laminar flows, since in this case the use of NS conditions is stabilizing [3]. Also, the influence of the confinement on the Strouhal number was examined in the turbulent regime, pointing out a difference of behaviour with respect to confined laminar wakes.

Depending on the confinement parameter, the turbulence has shown either 3D features or 2D ones. This dependence has been analyzed by looking both at the third order-velocity structure function and Lumley diagrams, with consistent results: For weak confinement the flow combines 2D/ 3D features, whereas for stronger confinements the turbulence is essentially 3D. This is enforced with NS rather than FS boundary conditions.

Although the confinement seems to favor the formation of a fully-developed 3D turbulence, especially when no-slip boundary

Please cite this article in press as: Biancofiore L et al. Influence of confinement on obstacle-free turbulent wakes. Comput Fluids (2012), doi:10.1016/j.compfluid.2011.12.008

conditions are involved, it would be of interest to study the role of the confinement for fully 2D flows, thus excluding artificially the transition to 3D flows. It is indeed not clear if our conclusions obtained for 3D flows also hold for 2D ones. The results of the present paper have been obtained in a channel like geometry. It would be interesting to understand if the confinement has the same influence on turbulent wakes also in an axisymmetric geometry, closer to a real coaxial injector. Furthermore, additional numerical or experimental studies devoted to confined laminar/ turbulent obstacle-free wakes could be conducted, in order to unveil the role of confinement on the appearance of laminar instability and 3D coherent structures, the transition to turbulence and its intensity.

Acknowledgements

For the numerical simulations carried out in this paper, we have used the support of the *Institut du Développement et des Ressources en Informatique Scientifique* (IDRIS) as a part of the project "Etude et contrôle de phénomènes tourbillonaires" (references i2009024055 and i2010024055), as well as the Mésocentre SIGAMM of the Observatory of Côte Azur as a part of the project "Instabilités de sillages". Stefano Musacchio (LJAD) and Eric Serre (M2P2, Marseille) are warmly acknowledged for stimulating discussions. The authors thank Jean-Marc Lacroix for his kindness and technical support.

Appendix A. Dissipation rates of the turbulent kinetic energy

We proceed as in Pasquetti [25], i.e. we compute the mean dissipation rate of the turbulent kinetic energy as, e.g. described in Pope [27], except that we start from the SVV-stabilized incompressible Navier–Stokes equations:

$$\partial_t \bar{u}_i + \bar{u}_j \partial_j \bar{u}_i = -\partial_i \bar{p} + \nu \partial_j \tilde{\partial}_j \bar{u}_i, \tag{14}$$

$$\partial_j \bar{u}_j = 0, \tag{15}$$

where summation over repeated indices is assumed, with $\tilde{\partial}_j$ as defined in Eq. (10) and, where $\bar{u}_i$ and $\bar{p}$ stand for the SVV–LES approximations of the i-component of the velocity and of the pressure divided by the density, respectively. The over-bar is a classical LES notation to express the fact that at the end we will only compute some filtered quantities, even if we have not followed the usual LES methodology, based on the filtered Navier–Stokes equations.

In order to obtain an equation for the specific kinetic energy of the filtered velocity, $e_f = \bar{u}_i \bar{u}_i/2$, we multiply Eq. (14) by $\bar{\mathbf{u}}$ and introduce the tensor $\widetilde{S}_{ij} = (\tilde{\partial}_j \bar{u}_i + \tilde{\partial}_i \bar{u}_j)/2$ which is associated to the work of the viscous and sub-grid forces

$$\overline{D}_t e_f + \partial_j (\bar{u}_j \bar{p} - 2\nu \bar{u}_i \widetilde{S}_{ij}) = -\epsilon, \tag{16}$$

with $\overline{D}_t = \partial_t + \bar{u}_j \partial_j$ and, where appears the dissipation term

$$\epsilon = \nu (\partial_j \bar{u}_i \tilde{\partial}_j \bar{u}_i + \partial_j (\bar{u}_i \tilde{\partial}_i \bar{u}_j)). \tag{17}$$

Assuming that ∂_j and $\tilde{\partial}_j$ commute, with the continuity equation and thanks to the symmetry of the $\widetilde{S}_{ij}$, one obtains:

$$\epsilon = 2\nu S_{ij} \widetilde{S}_{ij}. \tag{18}$$

Without SVV stabilization, thus, $\tilde{\partial}_j \equiv \partial_j$ and $\widetilde{S}_{ij} = S_{ij}$, we recover the usual form of the dissipation term. However, it should be noted that $S_{ij} S_{ij} \geqslant 0$, whereas ϵ, from Eq. (18), may be negative, giving then the possibility of a local transfer of energy from the non-resolved to the resolved scales. Such a backscatter like phenomenon may however be more numerical than physical, see e.g. the SGS Cholet and Lesieur [7] model for a more physical approach. The SVV stabilization however allows such a backscatter phenomenon, whereas some SGS models, e.g. the standard Smagorinsky model, forbid it.

From Eq. (18), it is possible to compute the dissipation rate of the turbulent kinetic energy. Hence, denoting with $\langle\cdot\rangle$ a statistical mean

$$\langle \epsilon \rangle = 2\nu \langle S_{ij} \rangle \langle \widetilde{S}_{ij} \rangle + \varepsilon, \tag{19}$$

where the first term in the right hand side is the dissipation due to the mean flow and ε the dissipation rate of the turbulent kinetic energy:

$$\varepsilon = 2\nu (\langle S_{ij} \widetilde{S}_{ij} \rangle - \langle S_{ij} \rangle \langle \widetilde{S}_{ij} \rangle). \tag{20}$$

Of course, with $\widetilde{S}_{ij} \equiv S_{ij}$ one recovers the standard formulation of ε, i.e. only based on the viscous dissipation. The validity of this approach was especially tested for the stratified wake of a cylinder [25].

References

[1] Bearman PW, Zdravkovich MM. Flow around a circular cylinder near a plane boundary. J Fluid Mech 1978;89:33–47.
[2] Bernard D. Three-point velocity correlation functions in two-dimensional forced turbulence. Phys Rev E 1999;60:6184.
[3] Biancofiore L. Influence of confinement on the spatiotemporal development of wakes. Ph.D. Thesis, Université de Nice-Sophia Antipolis; 2011.
[4] Biancofiore L, Gallaire F. Influence of shear layer thickness on the stability of confined two-dimensional wakes. Phys Fluids 2011;23:034103.
[5] Biancofiore L, Gallaire F, Pasquetti R. Influence of confinement on a two-dimensional wake. J Fluid Mech 2011;688:297–320.
[6] Boffetta G, Musacchio S. Evidence for the double cascade scenario in two-dimensional turbulence. Phys Rev E 2010;82:6307.
[7] Cholet J-P, Lesieur M. Parametrization of small scales of three dimensional isotropic turbulence utilizing spectral closures. J Atmos Sci 1981;38:2747–57.
[8] Cousin L, Pasquetti R. High-order methods for the simulation of transitional to turbulent wakes. In: Advances in scientific computing and applications. Beijing (New York): Science Press; 2004. p. 133–43.
[9] Gill GS. A qualitative technique for concentric tube element optimization, utilizing the factor/dynamic head ratio 1. AIAA paper 16–18, 1978.
[10] Hughes TJR, Mazzei L, Oberai AA. The multiscale formulation of large eddy simulation: Decay of homogeneous isotropic turbulence. Phys Fluids 2001;13(2):505–12.
[11] Juniper MP. Structure and stabilization of cryogenic spray flames. Ph.D. Thesis, École centrale Paris; 2001.
[12] Juniper MP. The effect of confinement on the stability of two-dimensional shear flows. J Fluid Mech 2006;565:171–95.
[13] Juniper MP, Candel S. The stability of ducted compound flows and consequences for the geometry of coaxial injectors. J Fluid Mech 2003;482:257–69.
[14] Karamanos GS, Karniadakis GE. A spectral vanishing viscosity method for large-eddy simulation. J Comput Phys 2000;163:22–50.
[15] Kim DH, Yang K-S, Senda M. Large eddy simulation of turbulent flow past a square cylinder confined in a channel. Comput Fluids 2004;33:81–96.
[16] Kraichnan RH. Inertial ranges in two-dimensional turbulence. Phys Fluids 1967;10:1417–23.
[17] Kraichnan RH. Inertial-range in two- and three-dimensional turbulence. J Fluid Mech 1971;47:525–35.
[18] Kraichnan RH, Montgomery D. Two-dimensional turbulence. Rep Prog Phys 1980;43:547–619.
[19] Lindborg E. Can the atmospheric kinetic energy spectrum be explained by two-dimensional turbulence? J Fluid Mech 1999;388:258–88.
[20] Lumley JL. Computational modeling of turbulent flows. Adv Appl Mech 1978;18:123.
[21] Maday Y, Ould Kaber SM, Tadmor E. Legendre pseudo-spectral viscosity method for nonlinear conservation laws. SIAM J Numer Anal 1993;30(2):321–42.
[22] Minguez M, Pasquetti R, Serre E. High-order large-eddy simulation of flow over a simplified car model. Phys Fluids 2008;20:095101.
[23] Pasquetti R. In: R. Pasquetti, Spectral vanishing viscosity method for LES: Sensitivity to the SVV control parameters, J. of Turbulence, vol. 6, N12, Special issue: Marseille Euromech Colloquium, 2004; 2005.
[24] Pasquetti R. Spectral vanishing viscosity method for large-eddy simulation of turbulent flows. J Sci Comput 2006;27:365–75.
[25] Pasquetti R. Spectral vanishing viscosity method for high-order LES: computation of the dissipation rates. In: Proceedings of "Computational Fluid Dynamics Conference ECCOMAS 2006", TU Delft, Netherlands; 2006.
[26] Pasquetti R. Temporal/spatial simulation of the stratified far wake of a sphere. Comput Fluids 2010;40:179–87.
[27] Pope SB. Turbulent Flows. Cambridge University Press; 2000.
[28] Rees SJ, Juniper MP. The effect of confinement on the stability of viscous planar jets and wakes. J Fluid Mech 2010;656:309–36.
[29] Rehab H, Villermaux E, Hopfinger EJ. Flow regimes of large-velocity-ratio coaxial jets. J Fluid Mech 1997;345:357–81.

Please cite this article in press as: Biancofiore L et al. Influence of confinement on obstacle-free turbulent wakes. Comput Fluids (2012), doi:10.1016/j.compfluid.2011.12.008

[30] Richter A, Naudascher E. Fluctuating forces on a rigid circular cylinder in confined flow. J Fluid Mech 1976;78:561–76.
[31] Sagaut P. Large-eddy simulation for incompressible flows: an introduction, series: scientific computation. Springer; 2005.
[32] Tammisola O, Lundell F, Schlatter P, Wehrfritz A, Södereberg LD. Global linear and nonlinear stability of viscous confined plane wakes with co-flow. J Fluid Mech 2011;675:397–434.
[33] Xu CJ, Pasquetti R. Stabilized spectral element computations of high Reynolds number incompressible flows. J Comput Phys 2004;196:680–704.
[34] Williamson CHK. Vortex dynamics in the cylinder wake. Annu Rev Fluid Mech 1996;28:477–539.

Please cite this article in press as: Biancofiore L et al. Influence of confinement on obstacle-free turbulent wakes. Comput Fluids (2012), doi:10.1016/j.compfluid.2011.12.008